

## Article

# Integration of Geochemical Modeling, Multivariate Analysis, and Irrigation Indices for Assessing Groundwater Quality in the Al-Jawf Basin, Yemen

Mohammed Hezam Al-Mashreki <sup>1</sup>, Mohamed Hamdy Eid <sup>2,3,\*</sup> , Omar Saeed <sup>1,4</sup>, András Székács <sup>4</sup> , Péter Szűcs <sup>2</sup>, Mohamed Gad <sup>5</sup> , Mostafa R. Abukhadra <sup>3,\*</sup> , Ali A. AlHammadi <sup>6,7</sup>, Mohammed Saleh Alrakhami <sup>1</sup>, Mubarak Ali Alshabibi <sup>1</sup>, Salah Elsayed <sup>8,9</sup> , Mosaad Khadr <sup>10,11</sup> , Mohamed Farouk <sup>12</sup>  and Hatem Saad Ramadan <sup>13</sup>

- <sup>1</sup> Renewable Natural Resources Research Center, Agricultural Research and Extension Authority, Dhamar P.O. Box 87148, Yemen
  - <sup>2</sup> Institute of Environmental Management, Faculty of Earth Science, University of Miskolc, 3515 Miskolc, Hungary
  - <sup>3</sup> Geology Department, Faculty of Science, Beni-Suef University, Beni-Suef 65211, Egypt
  - <sup>4</sup> Doctoral School of Environmental Science, The Hungarian University of Agriculture and Life Sciences, Páter Károly u. 1, 2100 Gödöllő, Hungary
  - <sup>5</sup> Hydrogeology, Evaluation of Natural Resources Department, Environmental Studies and Research Institute, University of Sadat City, Minufiya 32897, Egypt
  - <sup>6</sup> Chemical Engineering Department, Khalifa University of Science and Technology, Abu Dhabi P.O. Box 127788, United Arab Emirates
  - <sup>7</sup> Center for Catalysis and Separation (CeCaS), Khalifa University of Science and Technology, Abu Dhabi P.O. Box 127788, United Arab Emirates
  - <sup>8</sup> Agricultural Engineering, Evaluation of Natural Resources Department, Environmental Studies and Research Institute, University of Sadat City, Minufiya 32897, Egypt
  - <sup>9</sup> New Era and Development in Civil Engineering Research Group, Scientific Research Center, Al-Ayen University, Thi-Qar, Nasiriyah 64001, Iraq
  - <sup>10</sup> Civil Engineering Department, College of Engineering, University of Bisha, Bisha 61922, Saudi Arabia
  - <sup>11</sup> Irrigation and Hydraulics Department, Faculty of Engineering, Tanta University, Tanta 31734, Egypt
  - <sup>12</sup> Agricultural Engineering, Surveying of Natural Resources in Environmental Systems Department, Environmental Studies and Research Institute, University of Sadat City, Menofia Governorate, Sadat City 32897, Egypt
  - <sup>13</sup> Faculty of Earth Science, Beni-Suef University, Beni-Suef 62511, Egypt
- \* Correspondence: mohamedhamdy@science.bsu.edu.eg (M.H.E.); abukhadra89@science.bsu.edu.eg (M.R.A.)



**Citation:** Al-Mashreki, M.H.; Eid, M.H.; Saeed, O.; Székács, A.; Szűcs, P.; Gad, M.; Abukhadra, M.R.; AlHammadi, A.A.; Alrakhami, M.S.; Alshabibi, M.A.; et al. Integration of Geochemical Modeling, Multivariate Analysis, and Irrigation Indices for Assessing Groundwater Quality in the Al-Jawf Basin, Yemen. *Water* **2023**, *15*, 1496. <https://doi.org/10.3390/w15081496>

Academic Editor: Thomas M. Missimer

Received: 25 February 2023

Revised: 6 April 2023

Accepted: 8 April 2023

Published: 11 April 2023



**Copyright:** © 2023 by the authors. Licensee MDPI, Basel, Switzerland. This article is an open access article distributed under the terms and conditions of the Creative Commons Attribution (CC BY) license (<https://creativecommons.org/licenses/by/4.0/>).

**Abstract:** Water quality monitoring is crucial in managing water resources and ensuring their safety for human use and environmental health. In the Al-Jawf Basin, we conducted a study on the Quaternary aquifer, where various techniques were utilized to evaluate, simulate, and predict the groundwater quality (GWQ) for irrigation. These techniques include water quality indices (IWQIs), geochemical modeling, multivariate statistical analysis, geographic information systems (GIS), and adaptive neuro-fuzzy inference systems (ANFIS). Physicochemical analysis was conducted on the collected groundwater samples to determine their composition. The results showed that the order of abundance of ions was  $\text{Ca}^{2+} > \text{Mg}^{2+} > \text{Na}^+ > \text{K}^+$  and  $\text{SO}_4^{2-} > \text{Cl}^- > \text{HCO}_3^- > \text{NO}_3^-$ . The assessment of groundwater quality for irrigation based on indices such as Irrigation water quality index (IWQI), sodium adsorption ratio (SAR), sodium percent (Na%), soluble sodium percentage (SSP), potential salinity (PS), and residual sodium carbonate RSC, which revealed moderate-to-severe restrictions in some samples. The Adaptive Neuro-Fuzzy Inference System (ANFIS) model was then used to predict the IWQIs with high accuracy during both the training and testing phases. Overall, these findings provide valuable information for decision-makers in water quality management and can aid in the sustainable development of water resources.

**Keywords:** water quality; hydrochemical facies; ANFIS models; Quaternary aquifer; Yemen

## 1. Introduction

Groundwater (GW) is a crucial natural resource for the socioeconomic development of nations, but agriculture is identified as its primary global consumer [1]. GW is essential for sustained growth in various sectors in the long term, and a reliable water supply is vital for the economy, industry, and agriculture, relying on favorable GW attributes such as extensive coverage and superior quality [2–5]. Unfortunately, groundwater quality (GWQ) has deteriorated significantly in the past few decades due to factors such as population growth, industrial and agricultural expansion, and the impact of climate change. Inadequate management of natural resources caused by poor coordination and strategy integration exacerbates the situation leading to water crises and quality issues in many nations, especially those with arid and semi-arid climates [2–4].

Yemen is located in a region prone to water shortage due to insufficient rainfall and poor distribution, making it one of the top ten countries with water scarcity [6]. Yemen is among the most severely water-stressed countries in the Middle East and faces a severe water crisis due to the over-extraction of GW, inadequate infrastructure, and poor management practices, leading to the rapid depletion of aquifers [7,8]. Water resources in Yemen are primarily used in agriculture, and recent conflicts have disrupted food production and access to safe drinking water. Many farmers have been forced to abandon their land because of a lack of water, while urban areas rely heavily on GW, and rural regions depend on wells and conventional water collection techniques [9]. The country has limited water resources, with 1.5 billion m<sup>3</sup> of renewable groundwater, 1.0 billion m<sup>3</sup> of surface water, and 3.4 billion m<sup>3</sup> of water demand [10]. Recent population growth, coupled with an increased demand for water for agricultural purposes, particularly farming, and the absence of rainfall, has resulted in the overuse of GW [11]. The growing population combined with water shortages poses substantial socioeconomic and political challenges to the country and threatens its environmental stability [12].

GW chemical composition results from long-term interactions with the surroundings, and geological, climatic, and human factors profoundly affect the types and levels of substances found in the GW [13,14]. Physical and chemical patterns resulting from geological and anthropogenic activities affect GW quality [15]. Recharging, aquifer metrics, contact time, and particular geochemical mechanisms such as mineral solubility, dissolution, and ion exchange processes influence the geochemical properties of the GW [16–18]. Statistical analysis, Piper diagrams, Gibbs diagrams, Chadha diagrams, and ion ratios are effective methods to analyze the chemical features of GW and the factors governing them [19–22]. Geochemical models can help compute chemical reactions occurring in GW systems, such as dissolution and precipitation of solids, ion exchange, and sorption by clay minerals [23–25]. Statistical correlation analysis, which is an appropriate method for determining connections between various physicochemical factors, may be a distinguishing step toward GWQ management. Moreover, multivariate techniques such as cluster analysis (CA) and principal component analysis (PCA) are useful for identifying important physicochemical properties and the relationships among these factors to comprehend the primary elements affecting the distribution of physicochemical water parameters [26–28].

The sustainability of irrigation water quality is a crucial area of research worldwide, and various studies have produced hydrochemical indices for comprehensive assessments. Irrigation water quality indices (IWQI) have emerged as the preferred method for evaluating water quality and have been developed by numerous scientists [2,13]. IWQIs depend on the quantity and type of salts present in the water, and concerns associated with water quality degradation include increased salinity, diminished permeability, and exposure to highly toxic ions. Various techniques have been employed to assess irrigation water quality, including the use of IWQIs. IWQIs combine several physicochemical elements to create a single value that represents the suitability of water quality for irrigation [27,29,30]. Several studies have focused on using IWQI and other indices such as SAR, Na%, SSP, PS, and RSC to evaluate the suitability of groundwater (GW) for irrigation [31,32]. Furthermore, GIS can aid in mitigating some of these problems, particularly by integrating a water quality

assessment methodology with a spatial analysis tool, which can substantially enhance the visualization of research findings [33].

However, conventional techniques for assessing water quality can be costly and labor-intensive, particularly for farmers in developing nations. To address this challenge, machine learning (ML) models have been increasingly used in recent years to predict IWQIs of aquifer systems using physical characteristics as features. ML has been used more frequently in recent years to evaluate water quality in numerous research studies due to its effectiveness in resolving intricate issues and highlighting how input and output data are related [34–36]. To predict IWQIs for irrigation, ANFIS was used in this study. ANFIS has been used in a variety of hydrological applications, including the simulation of runoff and rainfall, stream flow prediction, and drought prediction [37–41]. These applications utilize the ability of ANFIS to model nonlinear and complex relationships between input and output variables, which is often the case in hydrological systems. One of the benefits of ANFIS in hydrology is its ability to handle uncertainty and imprecision in input data. This is achieved using fuzzy logic, which allows for the representation of vague and uncertain information in a mathematically tractable form. In addition, ANFIS can be easily integrated with other computational tools, such as evolutionary algorithms and swarm intelligence methods, to further improve its performance [42–44]. A decline in the quality of drinking water negatively impacts human health and the sustainable development of society. This problem has worsened in many regions owing to urbanization and population growth, leading to increased groundwater contamination. This contamination is mainly caused by the mismanagement of groundwater resources and the release of sewage from households and industries into the groundwater system. Contaminants in shallow aquifers can deteriorate deep aquifers and change geochemical conditions along this pathway [45,46].

Consequently, the purposes of this study were to: (1) study the characterization of GW in the Al-Jawf region, water types, and their geochemical processes; (2) determine the chemical composition of the GW used for irrigation in the Al-Jawf Basin; (3) evaluate the suitability of GW for irrigation across the Quaternary aquifer in the Al-Jawf Basin using IWQIs such as IWQI, SAR, Na %, SSP, PS, and RSC; and (4) evaluate the effectiveness of ANFIS modeling for the reliable prediction of IWQIs.

## 2. Materials and Methods

### 2.1. Site Descriptions and Hydrogeological Settings

The Al-Jawf Governorate is a province located in northwest Yemen, along the border with Saudi Arabia, approximately 170 km from Sana'a, the capital of Yemen. With an area of about 30,620 square kilometers and a population of around 663,147 people [47], it is administratively divided into twelve districts: Alhazm, Khab, and Alsha'af; Alghayl, Alkhalq, Barat Aleinan, Rajoozah, Kharab Almarashi, Almasloob, Almutun, Alzahir, Alhamidat, and Almatamah. The economy of the governorate is predominantly agricultural, with crops such as wheat, corn, fodder, and barley, and it also has small-scale industries such as textiles and food processing. The terrain of the Al-Jawf Governorate is characterized by plains, as it overlaps with the desert of the Empty Quarter and has a desert climate [48].

The study area is located in the northwestern part of Al-Jawf Governorate and includes five districts: Almasloob, Almutun, Alzahir, Alhamidat, and Almatamah. It is situated between the longitudes of 44°20'–44°40' E and the latitudes of 16°10'–16°20' N (Figure 1). The depth of the sampling wells ranged from 18 to 150 m below the ground's surface and penetrated the shallow Quaternary aquifer, which is unconfined and consists of sand intercalated with clays and carbonates [49].

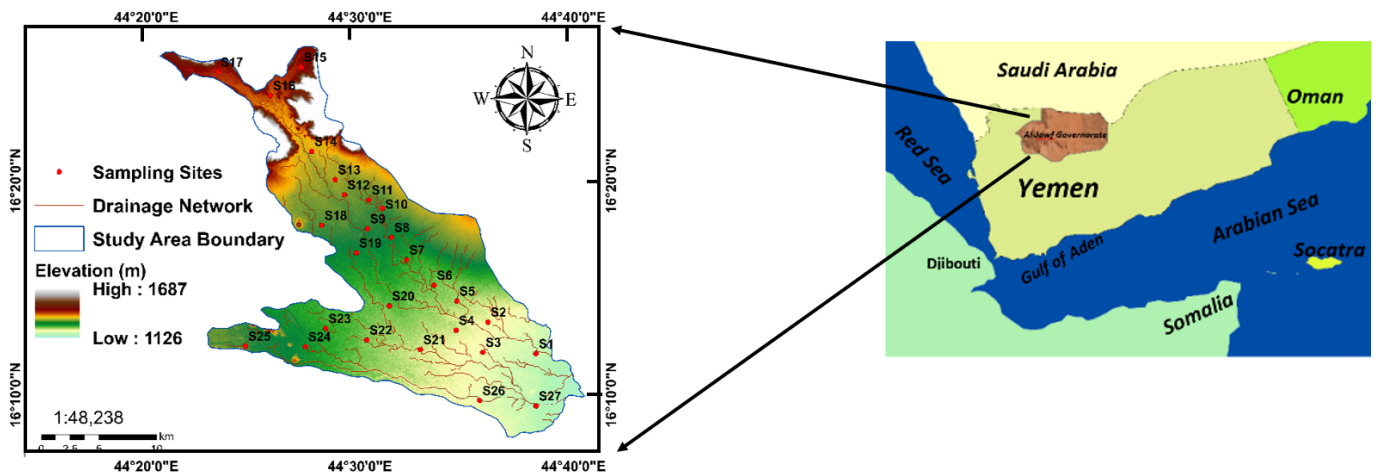


Figure 1. Location map and sampling sites of the research study area.

2.2. Geological and Hydrogeological Settings

According to Alaug [49], the subsurface geology of the Al-Jawf Basin is composed of a sedimentary succession that is characterized by alternating transgressive and regressive depositional cycles. These successions resulted from different rift phases and consisted of clastic rocks and carbonates. The succession can be summarized from youngest to oldest, as shown in (Figure 2). The Quaternary deposits in the region include the untied Tawilah Group (Cretaceous), Nayfa Formation (Berriasian-Hauterivian), Madbi Formation (Kimmeridgian), Shuqra Formation (Bathonian-Oxfordian), Kuhlan Formation (Early Middle Jurassic), and Wajid and/or Akbara Formations (Paleozoic) [49].

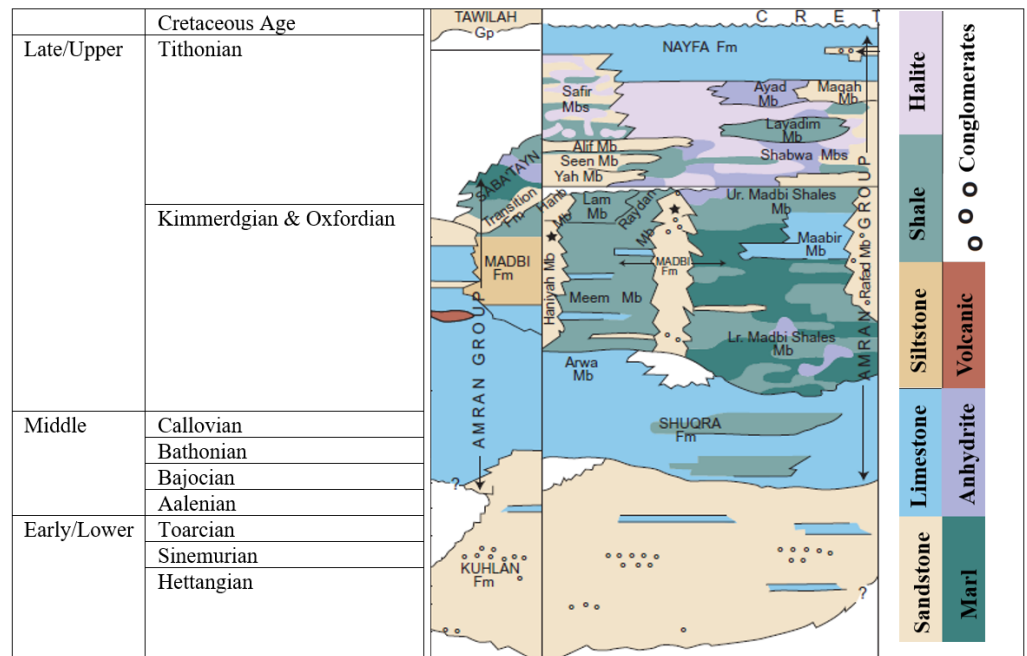


Figure 2. Geological, Hydrogeological units in the study area.

The elevation of the water level in this region ranges from 1089 to 1247 m above sea level, and the GW flows from northwest to southeast. However, excessive abstraction of GW in the central part of the study area has led to a rapid decrease in the water level, as seen on the map as a cone of depression from the local flow direction (Figure 3). The Wadi Al-Jawf region is known for its low rainfall rates, which means that there is limited GW recharge from precipitation. Instead, the main source of GW recharge in this area is

believed to be surface water, which flows from neighboring mountainous regions into the valleys and plains. This surface flow then percolates into the ground, replenishing the GW aquifers. This method is referred to as the diffuse recharge method and is a vital recharge source in arid and semi-arid regions with low precipitation rates. However, this method is less consistent and depends on the intensity of precipitation in mountainous areas and the effectiveness of infiltration. The main aquifer in the current study is composed of sandstone intercalated with shale, clay, and carbonate minerals such as limestone [49].

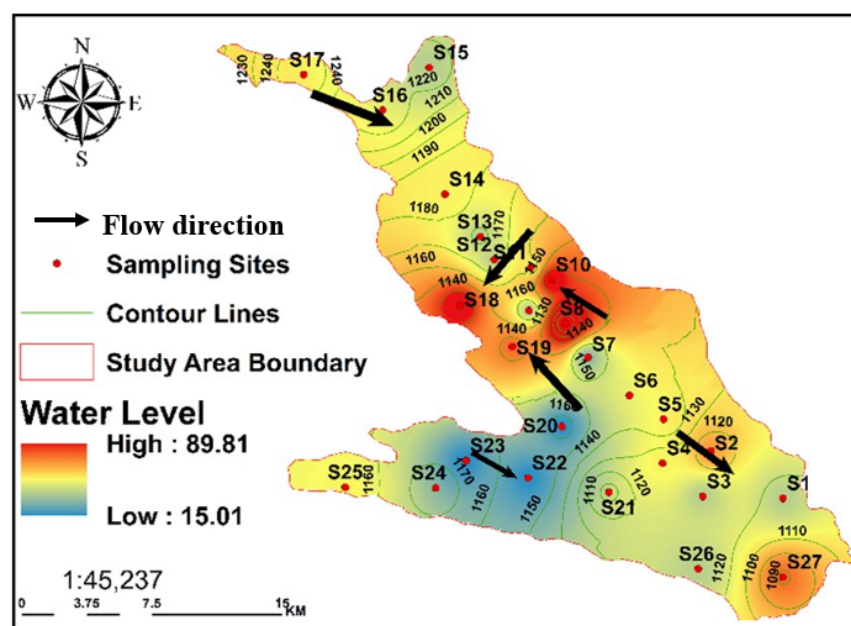


Figure 3. The Quaternary aquifer's groundwater flow direction.

### 2.3. Water Sampling and Analysis

The groundwater samples, totaling 27, were collected from wells and boreholes located throughout the Quaternary Aquifer in the Al-Jawf region. Non-acidified water samples were collected and stored in approximately 1.5 dm<sup>3</sup> polyethylene bottles, which were then kept at 4 °C. The chemical composition of the water was analyzed to determine the presence of Mg<sup>2+</sup>, Ca<sup>2+</sup>, K<sup>+</sup>, Na<sup>+</sup>, SO<sub>4</sub><sup>2-</sup>, HCO<sub>3</sub><sup>-</sup>, Cl<sup>-</sup>, and NO<sub>3</sub><sup>-</sup>. The ionic balance (IB) was calculated as a percentage difference between the total amount of positively charged ions (cations) and negatively charged ions (anions) present in water using the following formula (Equation (1)):

$$IB = (TC - TA)/(TC + TA) \times 100 \quad (1)$$

where TC represents the total amount of cations and TA represents the total amount of anions, both measured in milliequivalents per liter. To confirm the assessment of water quality, an acceptable range for IB is within  $\pm 5$  [50].

Water analyses were conducted in May 2021 using the following procedures: Bicarbonates were determined by titration with the methyl orange endpoint immediately upon sampling. The chloride content was estimated using Mohr titration and precipitation of AgCl until the appearance of silver chromate [51]. The nephelometric technique was used to calculate sulfate [52], while colorimetric analysis was performed to examine the nitrates [53]. Complex metric titration was used to estimate the amounts of calcium and magnesium, and emission spectrometry was used to measure the concentrations of Na and K [51].

### 2.4. Multivariate Statistical Methods and Data Treatments

#### 2.4.1. Cluster Analysis

CA is an unsupervised pattern recognition approach that classifies an enormous volume of data from each entity into multiple clusters and identifies the characteristics of

each group [54,55]. It is frequently used for hydrochemical investigations to categorize hydrogeochemical processes in groundwater by grouping collected water samples into significant geological and hydrogeological groups [56]. The outcomes of CA are displayed in a dendrogram [57], which considerably reduces the complexity of the original data while still showing the groupings and their closeness, providing a visual picture of the clustering activities [58].

#### 2.4.2. Principal Component Analysis/Factor Analysis

PCA is a linear structure used for analyzing complex multivariate datasets statistically without losing information [59]. It is a method of compressing data and estimating the number of variables required to elucidate observed fluctuations in the data. PCA can reduce the number of variables required while still capturing the same amount of variation with fewer variables [60]. The PC that contributes significantly to illustrating the variance in the measured data in traditional PCA has a greater eigenvalue. Moreover, PCA helps in comprehending the relationships between fundamental and indirect observable aspects of data [61].

### 2.5. Indexing Approach

#### 2.5.1. Index of the Processes Influencing Groundwater Chemistry

Another approach to identifying the origin and interrelationships among major elements is by using  $[\text{SO}_4^{2-}]$  versus  $[\text{Ca}^{2+}]$ ,  $[\text{HCO}_3^- + \text{SO}_4^{2-}]$  versus  $[\text{Ca}^{2+} + \text{Mg}^{2+}]$ ,  $[\text{Na}^+]$  versus  $[\text{Cl}^-]$ , and  $[\text{HCO}_3^-]$  versus  $[\text{Ca}^{2+} + \text{Mg}^{2+}]$ . The chloralkaline indices (CAI-I and CAI-II) (Equations (2) and (3)) were used in this study to determine the minerals in the aquifers and GW-exchange ions [62].

$$\text{CAI - I} = \frac{\text{Cl}^- - (\text{Na}^+ + \text{K}^+)}{\text{Cl}^-} \quad (2)$$

$$\text{CAI - II} = \frac{\text{Cl}^- - (\text{Na}^+ + \text{K}^+)}{\text{SO}_4^{2-} + \text{HCO}_3^- + \text{CO}_3^{2-} + \text{NO}_3^{2-}} \quad (3)$$

#### 2.5.2. Saturation Index (SI)

Additionally, a speciation model was used to determine the saturation index (SI) of minerals in GW samples from the Al-Jawf Basin. The SI of a mineral indicates its saturation level relative to the surrounding system. It was used in this study to predict the presence of reactive minerals in aquifers based on water samples without requiring solid-phase samples or mineral analysis [63].

Equation (4) was used to calculate the SI;

$$\text{SI} = \log (\text{IAP}/\text{K}_{\text{sp}}) \quad (4)$$

IAP expresses for “ion activity product,” and  $\text{K}_{\text{sp}}$  expresses for “solubility product” at a particular temperature. An SI of 0 indicates that the water is saturated and in equilibrium with the minerals; a positive value indicates oversaturation, and a negative value represents undersaturation.

#### 2.5.3. Irrigation water Quality Indices (IWQIs)

The physicochemical characteristics of the GW were used to compute the six IWQIs, as shown in Table 1.

**Table 1.** The calculation methods of the irrigation indices.

IWQIs	Formula	References
IWQI	$\sum_{i=1}^n Q_i \times W_i$	[31]
SAR	$\left( \frac{Na^+}{\sqrt{(Ca^{2+} + Mg^{2+})/2}} \right) \times 100$	[64]
Na %	$\frac{(Na^+ + K^+)}{(Ca^{2+} + Mg^{2+}) + (Na^+ + K^+)} \times 100$	[65]
SSP	$\frac{Na^+}{Ca^{2+} + Mg^{2+} + Na^+} \times 100$	[66]
PS	$Cl^- + \left( \frac{SO_4^{2-}}{2} \right)$	[67]
RSC	$(HCO_3^- + CO_3^-) - (Ca^{2+} + Mg^{2+})$	[66]

Note: The IWQIs are determined in meq/L, except IWQI in mg/L.

**Irrigation Water Quality Index (IWQI)**

The EC, SAR, Na<sup>+</sup>, Cl<sup>-</sup>, and HCO<sub>3</sub><sup>-</sup> variables were used to generate the non-dimensional IWQI scale (Equations (5)–(7)), which has a range of 0–100 [31].

$$IWQI = \sum_{i=1}^n Q_i \times W_i \tag{5}$$

where Q<sub>i</sub> is the value of the quality measurement according to the tolerance thresholds, and W<sub>i</sub> is the set weight of each parameter (Table 2).

$$Q_i = Q_{max} - \left( \frac{[(X_{ij} - X_{inf}) \times Q_{imap}]}{X_{amp}} \right) \tag{6}$$

where X<sub>inf</sub> is the value that matches the lower limit of the class, X<sub>ij</sub> is the observed value for each parameter, Q<sub>imap</sub> is the class amplitude, and X<sub>amp</sub> is the amplitude class within which the parameter falls.

**Table 2.** The range of limit values of the parameters used in the computation of quality measurement (Q<sub>i</sub>).

Q <sub>i</sub>	SAR	EC (µs/cm)	HCO <sub>3</sub> <sup>-</sup> (meq/L)	Na <sup>+</sup> (meq/L)	Cl <sup>-</sup> (meq/L)	HCO <sub>3</sub> <sup>-</sup> (meq/L)
0–35	SAR > 2 or SAR ≥ 12	EC < 200 or EC ≥ 3000	HCO <sub>3</sub> <sup>-</sup> < 1 or HCO <sub>3</sub> <sup>-</sup> ≥ 8.5	Na < 2 or SAR ≥ 9	Cl < 1 or Cl ≥ 10	HCO <sub>3</sub> <sup>-</sup> < 1 or HCO <sub>3</sub> <sup>-</sup> ≥ 8.5
35–60	6 ≤ EC < 12	1500 ≤ EC < 3000	4.5 ≤ HCO <sub>3</sub> <sup>-</sup> < 8.5	6 ≤ Na < 9	7 ≤ Cl < 10	4.5 ≤ HCO <sub>3</sub> <sup>-</sup> < 8.5
60–85	3 ≤ EC < 6	750 ≤ EC < 1500	1.5 ≤ HCO <sub>3</sub> <sup>-</sup> < 4.5	3 ≤ Na < 6	4 ≤ Cl < 7	1.5 ≤ HCO <sub>3</sub> <sup>-</sup> < 4.5
85–100	2 ≤ EC < 3	200 ≤ EC < 750	1 ≤ HCO <sub>3</sub> <sup>-</sup> < 1.5	2 ≤ Na < 3	1 ≤ Cl < 4	1 ≤ HCO <sub>3</sub> <sup>-</sup> < 1.5

Finally, Equation (6) was used to obtain the W<sub>i</sub> values:

$$W_i = \frac{\sum_{j=1}^k F_j A_{ij}}{\sum_{j=1}^k \sum_{i=1}^n F_j A_{ij}} \tag{7}$$

where i represents the account of physicochemical variables selected by the model, with a range of 1 to n, j is the number of factors selected by the model, between 1 and k, and F is the auto value of component 1. A = parameter i substantially limited by factor j.

**2.6. Adaptive Neuro-Fuzzy Inference System (ANFIS)**

An ANFIS is an artificial neural network that uses fuzzy logic to make decisions [68,69]. It integrates the learning ability of a neural network with its ability to interpret fuzzy logic.

ANFIS is used for both classification and regression tasks and can be used to simulate intricate nonlinear input-output interactions. The methodology of using ANFIS can be divided into several steps [70–72].

1. Model design: In this step, the ANFIS model is designed, including the number of input and output variables, the number of fuzzy rules, and the structure of the adaptive network layer. Based on the complexity of the interactions between the input and output variables, the structure of the ANFIS model can be selected, and the number of fuzzy rules can be determined according to the number of input variables and the desired level of detail in the model;
2. Fuzzy partitioning: In this step, the input space is divided into a set of fuzzy regions using fuzzy partitioning techniques such as clustering or grid partitioning. The objective of fuzzy partitioning is to divide the input space into regions such that the input variables in each region are similar with respect to their relationships with the output variable;
3. Rule-based generation: In this step, a set of fuzzy rules is generated based on fuzzy partitions and relationships between the input and output variables. Each fuzzy rule consists of an antecedent (the if part of the rule) and a consequent (the then part of the rule), and the antecedent typically consists of a set of fuzzy membership functions that describe the relationship between the input variables and fuzzy regions;
4. Model training: In this step, the ANFIS model is trained using a set of training data and an optimization algorithm, such as gradient descent or particle swarm optimization, to adjust the model parameters and improve performance. The objective of the training is to minimize the error between the predicted and observed output values, which can be achieved using a variety of optimization algorithms and loss functions.

The relationships between IWQIs and water quality measures were established using ANFIS and represented as fuzzy if-then rules (Figure 4). The ANFIS models employed Sugeno-type FIS of a bell as input membership functions, with five functions. However, the outputs had linear membership functions. Figure 5 illustrates the ANFIS model, which includes a multilayer feedforward architecture and incoherent x- and y-input networks.

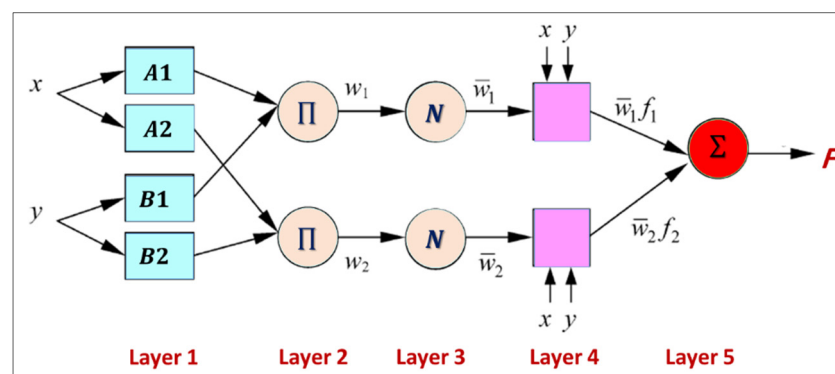


Figure 4. ANFIS system with a two-rule Sugeno system.

This study utilized ANFIS to determine the relationships between IWQIs and water quality metrics. The relationships between IWQIs and water quality parameters were described as if-then fuzzy rules, which can predict IWQIs based on input variables (Figure 5). The rule foundation of the Sugeno model (Figure 5) is as follows (Equations (8) and (9)):

$$\text{If } a = A_1 \text{ and } b = B_1 \text{ we have } f_1 = p_1 \times a + q_1 \times b + r_1 \tag{8}$$

$$\text{While, if } a = A_2 \text{ and } b = B_2 \text{ we have } f_2 = p_2 \times a + q_2 \times b + r_2 \tag{9}$$

The ANFIS system consists of five layers, as shown in Figure 6. The membership functions for fuzzy sets A and B are denoted by  $\mu A_i$  and  $\mu B_i$ , respectively. A and

B are orders of magnitude, and a and b are indicators of indirect identification function. The forward pass of the training algorithm modifies the relevant constraints p, q, and r, whereas output  $f_i$  falls within an inconsistent region defined by the FIS concept. Khadr [28] provided additional information on the ANFIS.

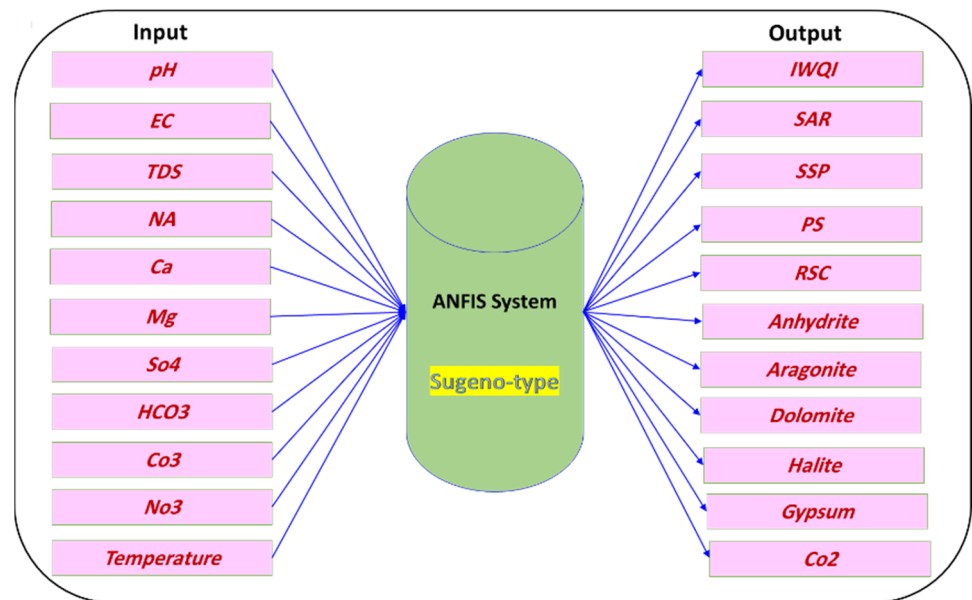


Figure 5. An ANFIS architecture for IWQ prediction.

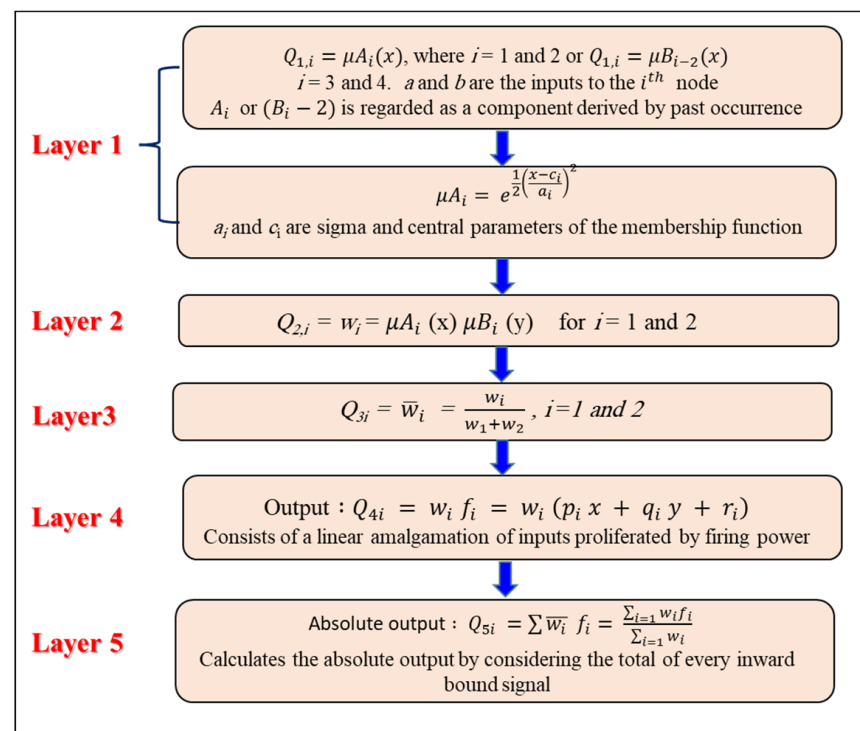


Figure 6. Conceptual illustration of the five layers that comprise ANFIS.

2.7. Performance Evaluation of the Simulation Models

To determine the accuracy and effectiveness of the ANFIS model for predicting the IWQs, several statistical measures were used for performance evaluation. These measures are commonly employed to compare the output of a model with the actual data

or the output of other models. They provided quantitative insights into the predictive capability, reliability, and accuracy of the model. These measures include the following (Equations (10)–(13)):

(a) Nash–Sutcliffe efficiency coefficient (NSE)

$$E = 1 - \left[ \frac{\sum_{i=1}^n (IW_{oi} - IW_{fi})^2}{\sum_{i=1}^n (IW_{oi} - IW_o)^2} \right] \tag{10}$$

(b) The mean absolute error (MAD)

$$MAD = \frac{\sum_{i=1}^n |IW_{oi} - IW_{fi}|}{n} \tag{11}$$

(c) The absolute variance fraction,  $R^2$

$$R^2 = 1 - \frac{\sum_{i=1}^n (IW_{oi} - IW_{fi})^2}{\sum_{i=1}^n (IW_{oi})^2} \tag{12}$$

(d) The root-mean-square error (RMSE)

$$RMSE = \sqrt{\frac{\sum_{i=1}^n (IW_{oi} - IW_{fi})^2}{n}} \tag{13}$$

$IW_o$  is the observed IWQ index,  $n$  is the number of data points,  $IW_f$  is the predicted IWQ index, and  $IW$  is the average observed Irrigation water quality index. Figure 7 illustrates the model architecture used by the ML algorithms.

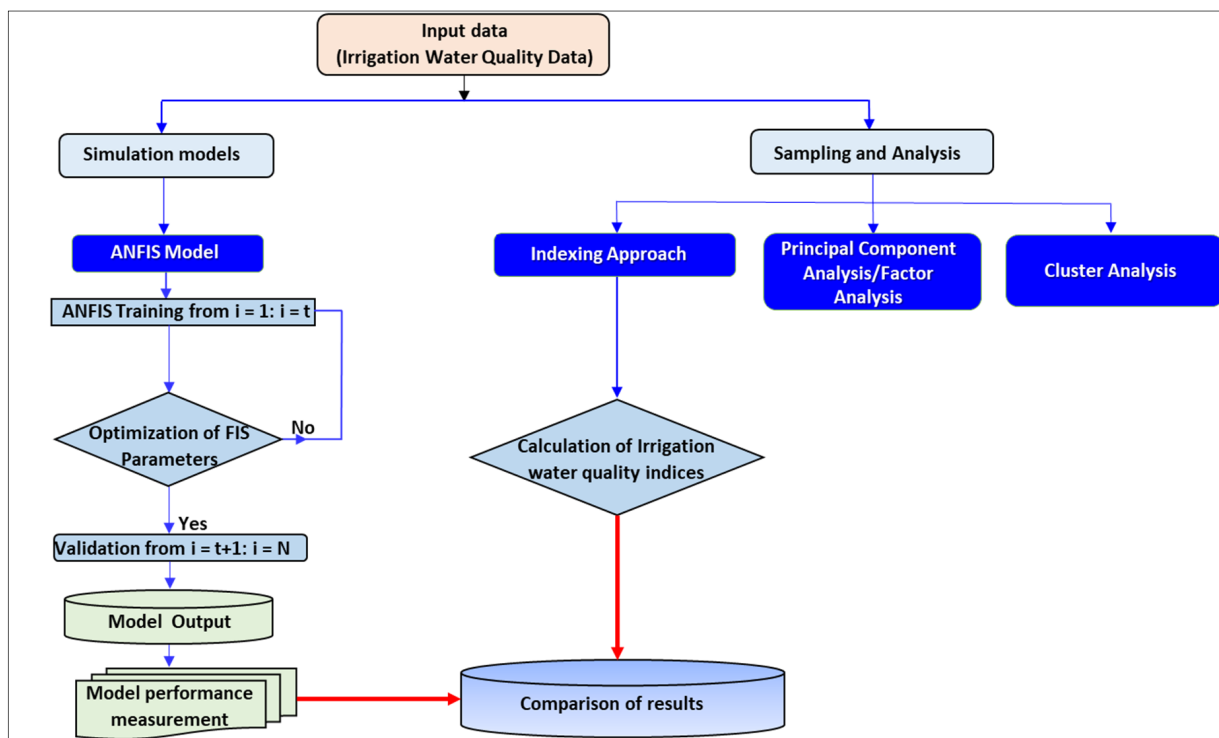


Figure 7. Schematic diagram of the methodology presented in this study.

### 2.8. Data Analysis, Processing, and Spatial Distribution

Statistical analyses were performed on the physicochemical characteristics and IWQIs using SPSS software version 22. According to the compositions of cations and anions, Piper, Chadha, and Gibbs diagrams were used to identify hydrogeochemical evolution and water types and to show the relationship between the characteristics of aquifers and water chemistry using OriginPro 2022 v.9.90 [21,73]. To identify the key elements in the water and improve water quality evaluation by simplifying the data analysis into understandable patterns, CA and PCA were utilized with the aid of statistical software (Version 8). These techniques enable the extraction of important information from large and complex datasets and facilitate the identification of underlying patterns and relationships among variables [74]. To establish the spatial relationships among the chemical properties of the data collected from various sample sites, several water quality indices (IWQIs) were developed. The purpose of these indices was to provide a framework for spatially connecting chemical properties. To visualize these indices, ArcGIS 10.5 was used to produce maps using raster interpolation and spatial analysis techniques, specifically the inverse distance weighted (IDW) method. IDW is generally a good choice when dealing with widely spaced data points or local variations in the data and when it is important to preserve abrupt changes in the data, which is the case in the current study. In contrast, kriging is better suited for smoothly varying data with a clear spatial correlation.

## 3. Results and Discussion

### 3.1. Hydrochemical Characteristics of Groundwater

The physicochemical characteristics of the Al-Jawf groundwater were examined to analyze the physicochemical quality of the Quaternary aquifer waters. Samples of GW had an average temperature of 20.7 °C. The pH of the water indicated that the type of terrain being traversed affected whether it was acidic or alkaline. TDS concentrations vary from 378.42 and 5012 mg/L. The GW samples may be classified as fresh to moderately saline by TDS, and 18.5% of them exceeded the FAO [75] water criteria. The measured water had a pH between 6.5 and 7.5, with a mean of 7.13. The FAO [75] standards were met based on these results (Table 3). The pH value also showed that the water was low in alkalinity and that the mechanisms that fix dolomite and calcite predominated between the pH values of 6.5 and 8.5. S19 well had the highest pH value, whereas S7 had the lowest.

**Table 3.** Descriptive results of the groundwater samples with the standard limit for irrigation purposes.

Parameter	Unit	FAO	Min	Max	Average
pH	-	8.5	6.5	7.5	7.13
Temp.	(°C)	-	11.5	27.1	20.7
TDS	(mg/L)	2000	378.42	5012	1685
EC	(µS/cm)	3000	542	6628	2361.72
Ca <sup>2+</sup>	(mg/L)	400	40	460	179.69
Mg <sup>2+</sup>	(mg/L)	60	32.81	328	114.5
K <sup>+</sup>	(mg/L)	2	2.34	23.40	9.54
Na <sup>+</sup>	(mg/L)	919	24.15	724.5	197.2
HCO <sub>3</sub> <sup>-</sup>	(mg/L)	610	150	915	408.18
Cl <sup>-</sup>	(mg/L)	1036	35.5	1136	395
SO <sub>4</sub> <sup>2-</sup>	(mg/L)	960	19.2	1939	392
NO <sub>3</sub> <sup>-</sup>	(mg/L)	10	0.1	6	2.21

As a result, the EC provides data on the degree of water mineralization. With a range of 542–6628 µS/cm, GW has an average EC of 2361.72 µS/cm. Notably, this study found results above the FAO recommendation of 3000 S/cm in 18.5% of the water samples [75]. All GW in the Al-Jawf region had higher EC ratings when the subsurface flows were directed toward the discharge areas southwest of Al-Jawf. The Ca<sup>2+</sup> levels in the water

samples ranged from 40 to 460 mg/L. For irrigation water, the FAO establishes a 400 mg/L maximum acceptable threshold. The average number of water sites was below the FAO recommendation, with  $Mg^{2+}$  concentrations ranging from 32.81 and 328 mg/L [75]. Water hardness is primarily caused by high amounts of alkaline earth elements. Soil type affected their concentrations. The amount of  $Ca^{2+}$  reached its peak towards the southeast and southwest. Similarly, the southeast and southwest of the Al Jawf area had the highest  $Mg^{2+}$  concentrations, reaching a maximum of 114.5 mg/L. The dolomites from the Cretaceous and Tawilah groups were altered and dissolved, resulting in this concentration. In general, the breakdown of dolomitic rocks ( $CaMg(CO_3)_2$ ), gypsum ( $CaSO_4$ ), and calcium carbonate ( $CaCO_3$ ) in the aquifer produces  $Ca^{2+}$  (Equations (14)–(16)):



The alkaline elements  $Na^+$  and  $K^+$  are naturally found in irrigation water and the Earth's crust. The  $Na^+$  concentration in the Al-Jawf GW varied from 24.15 to 724.5 mg/L. All the examined water samples were below the FAO limit of 919 mg/L [75]. The  $K^+$  concentrations ranged from 2.34 to 23.40 mg/L. The Food and Agriculture Organization (FAO) standard establishes a maximum permissible concentration of 2 mg/L for irrigation water. The breakdown of KCl and NaCl in rock-water interactions, saline seeps, and minor air inputs are the causes of this enrichment [76]. The highest potassium concentrations were found in samples collected from wells in the central and southern parts of the study area.

The concentration of  $Cl^-$  ranged from 35.5 to 1136 mg/L, with the latter being the maximum value. A previous study [52] suggested that the high chloride concentration could be due to the types of formations through which the water passes, or it may be a result of inadequate sewage waste treatment. Some numbers do not meet the FAO requirements (1036 mg/L) [75]. In the water boreholes, the highest  $Cl^-$  concentrations were found in two samples from the southwest of the study area. High  $Cl^-$  concentrations make metals rust, make water taste salty, and reduce the strength of concrete.

The FAO guidelines [75] state that the  $HCO_3^-$  concentration should be approximately 610 mg/L. Nevertheless, the GW samples from the study area revealed levels between 150 and 915 mg/L, which fell within the previously specified range, except for four samples that exceeded the limit. The samples with the highest  $HCO_3^-$  contents were S7, S17, S22, and S23, with values of 915, 730, 780, and 823.5 mg/L. In this study,  $SO_4^{2-}$  levels varied from 19.2 and 1939 mg/L and complied with FAO standards except for two samples in the southwest of the Al-Jawf region that exceeded the limits [75]. The use of chemical fertilizers by farmers, which is an intensive agricultural practice, has led to an increase in the concentration of  $SO_4^{2-}$  [77]. High concentrations of sulfate in irrigation water can seriously harm public health [78]. In the southwestern part of the research area,  $SO_4^{2-}$  concentrations were the highest. These typically increase in the direction of the subsurface flow. The gypsum and anhydrite in the mineral dissolved, resulting in the highest  $SO_4^{2-}$  concentrations. Sulfate ions can also be derived from the weathering of sulfide minerals such as pyrite, which requires further investigation to confirm the presence of pyrite in the aquifer [79].

The water samples analyzed in the Al-Jawf region had  $NO_3^-$  concentrations ranging from 0.1 to 6 mg/L. These values were below the recommended FAO range (10 mg/L) [75]. According to Table 3, the low value of nitrates in the study area indicates that there was no nitrate contamination from anthropogenic activities. Figure 8 shows the distribution maps of the physicochemical parameters in the study area.

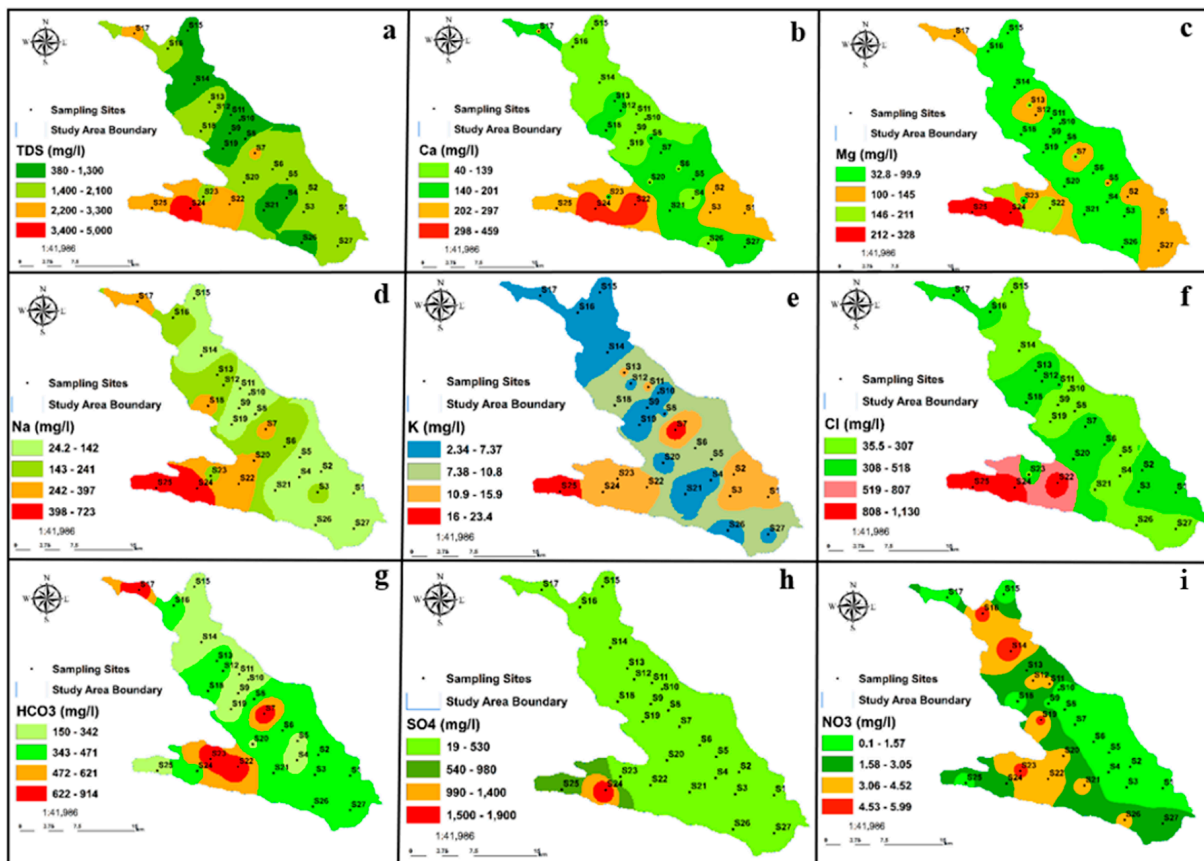


**Figure 8.** Distribution map of the physicochemical parameters: (a) TDS, (b)  $\text{Ca}^{2+}$ , (c)  $\text{Mg}^{2+}$ , (d)  $\text{Na}^+$ , (e)  $\text{K}^+$ , (f)  $\text{Cl}^-$ , (g)  $\text{HCO}_3^-$ , (h)  $\text{SO}_4^{2-}$ , and (i)  $\text{NO}_3^-$ .

### 3.2. Groundwater Facies and Processes Influencing Groundwater Chemistry

Hydrochemical processes occurring in aquifers may affect groundwater chemistry [80]. The distribution of groundwater facies is primarily attributed to local geology and lithology, particularly in arid to semi-arid regions [81]. Major ions regulate hydrochemical processes, which is why Chadha's diagram and the Piper diagram [20,22] were employed in this study (Figure 9a,b). The relative composition of the GW can be determined based on cation-anion pairings and the position of the plot [82]. Most of the samples used in this investigation fell into Field 3, and only two samples fell into Field 2 in Chadha's diagram (Figure 9b). In the Piper diagram (Figure 9a), 25 samples fell into zone 1 and two samples into zone 2 of the diamond shape. Both diagrams confirm the same water type, which is represented by the Ca-Mg-Cl/ $\text{SO}_4$  type and Ca-Mg- $\text{HCO}_3$  type, respectively, where alkaline metals are more abundant than alkaline earth metals and weakly acidic anions are more prevalent than strongly acidic anions. Several diagrams have been used by different researchers to determine the chemical composition of groundwater or water types, such as the TIS salinity diagram [83], ionic ratio relationships, Chadha's diagram, and the Piper diagram. Ionic ratios, gibbs diagram, and chadha's diagram were applied alongside the Piper diagram to show the geochemical evolution of groundwater from the recharge area to the discharge area. The results revealed that the water type in the recharge area was Ca-Mg- $\text{HCO}_3$ , and during the flow and water-rock interaction, the water type changed to Ca-Mg-Cl/ $\text{SO}_4$  in the discharge zone. Furthermore, saturation indices could reflect the mineral composition of the aquifer. A Gibbs diagram could reflect the relationship between the ionic ratio and salinity.

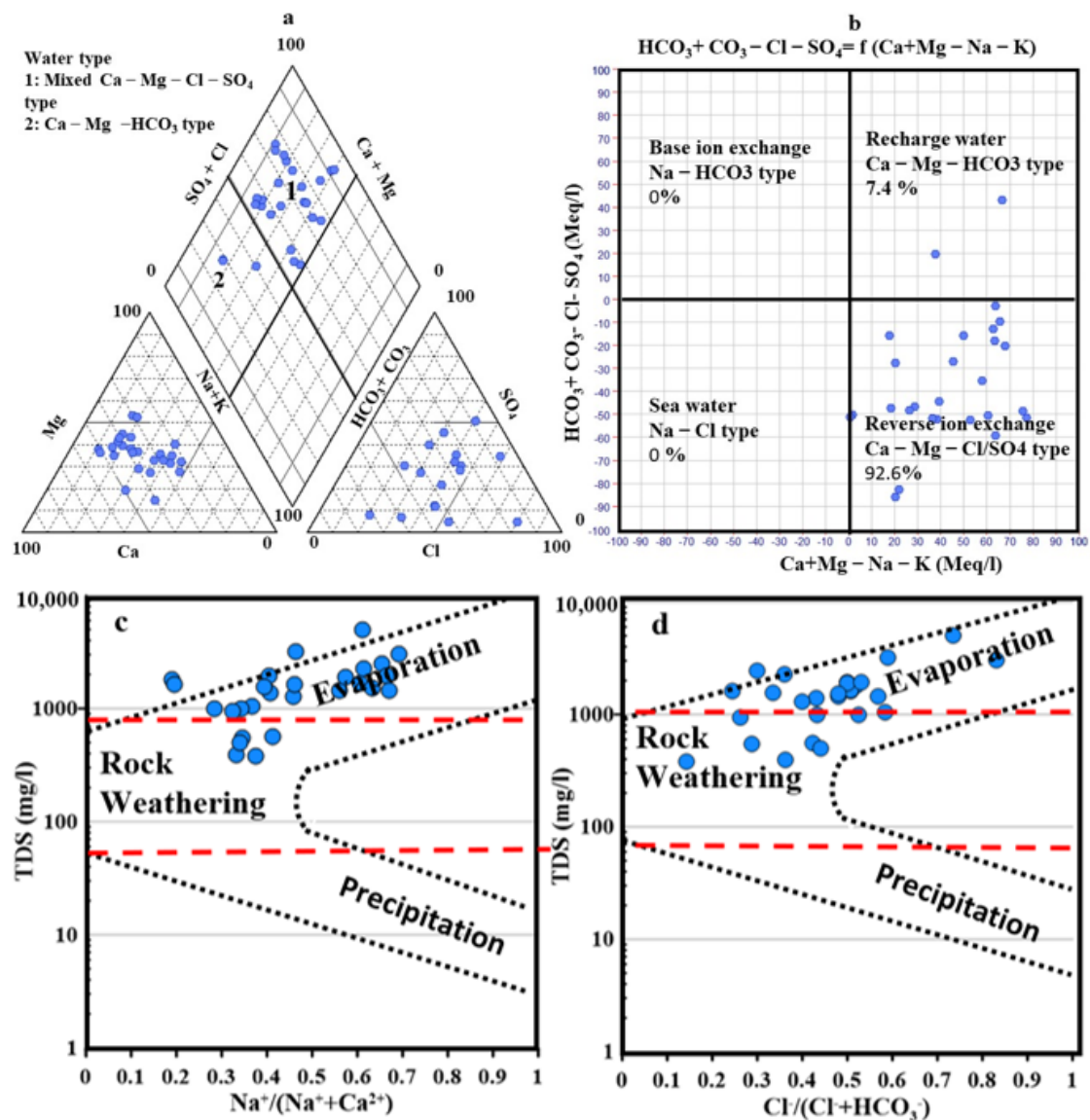
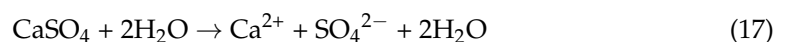


Figure 9. Plotting water samples on piper diagram (a), Chadha diagram (b), (c,d) Gibbs diagram.

Analysis of the local concentrations of several elements revealed that the cations developed as follows:  $Ca^{2+} > Mg^{2+} > Na^+ > K^+$ , whereas the anion evolution was as follows:  $SO_4^{2-} > Cl^- > HCO_3^- > NO_3^-$ . The breakdown of evaporitic deposits revealed calcium and magnesium sulfate facies in the chemical profile. The lithology of the region and anthropogenic factors, such as unrestricted fertilization and irrigation water quality, significantly affect the distribution of major ions ( $Ca^{2+}$ ,  $Mg^{2+}$ , and  $SO_4^{2-}$ ). Calcium and magnesium sulfates can provide both calcium and magnesium upon breakdown. Nevertheless, the change from one dominant ion to another might have been caused by dilution following the mixing or precipitation of one of the ions.

The two primary sources of  $SO_4^{2-}$  that have been identified are organic matter decomposition in the soil and the addition of leachable organic matter in the highly intensively cultivated regions of the Al-Jawf plain. The dissolution of gypsum is also recognized as a secondary source of sulfate [84]. According to Equation (17), the evaporite sequence's existence permits the dissolution of gypsum.



The fundamental mechanisms governing the evolution of water and the numerous hydrogeochemical processes affecting GW chemistry in the study region were examined using Gibbs plots [21]. Evaporation and rock weathering are significant components in the evolution of water chemistry, as shown by the Gibbs plots (Figure 9c,d), which show that the majority of the GW samples under study lie in the top portion of the diagrams (evaporation-dominant), and five samples fall in the rock weathering zone.

Figure 9c,d shows that the evaporation process is responsible for the plots' redirection to the Al-Jawf plain's evaporation dominance zone, which is located in a region with an arid climate and shallow GW depth. However, human activity can also affect the groundwater hydrochemical evolutionary processes, which Gibbs diagrams cannot explain [85].

Nonetheless, the shallow water depth in the area was related to the improvement in water levels caused by increased irrigation and effective rainfall. The ion concentrations were primarily influenced by evaporation. In addition, the approaching saturated zone is particularly wet and rich in evaporites, which causes the evaporites to precipitate through evaporation and ultimately leak into the saturated zone. The upshot of this is an increase in salinity ( $TDS_{max} = 5012$  mg/L) as evaporation from the earth becomes more severe as the water level increases, and sulfate GW is more influenced by evaporation than bicarbonate GW [86]. These results are complemented by other experiments that demonstrated that the sulfate-type GW in the alluvial plain is subject to high evaporation [87].

The lack of a balanced association between  $Na^+$  and  $Cl^-$  ions indicated that there was no equilibrium between them. This could be attributed to the prevalent sources of these ions, including halite dissolution. Only a few samples fell on the 1:1 line graph (Figure 10a). The majority of the samples fell below the 1:1 line graph, suggesting an excess of chloride, indicating either an additional source of chloride ions or the removal of  $Na^+$  from the GW via ion exchange. The high levels of chloride might be ascribed to human activities such as waste disposal, seepage of excess irrigated water from agricultural land, or deposition of chloride from the atmosphere. Anthropogenic disturbances, rather than variability in climate parameters, have been identified as the primary cause of surface freshwater shortage in the country, rather than variability in climate parameters [88]. Both reverse ion exchange and ion exchange have an impact on aquifer chemistry in the research region of Al-Jawf, as illustrated in Figure 10b through the scatter plot between  $Ca^{2+} + Mg^{2+}$  and  $HCO_3^- + SO_4^{2-}$ . The samples that were close to the 1:1 line demonstrated that the most frequent reactions in the research region system were calcite, dolomite, and gypsum dissolution. However, below the 1:1 line, the ion exchange mechanism is evident, with  $Ca^{2+}$  remaining in the soil and  $Na^+$  returning to the GW. In contrast, those above line 1:1 show reverse ion exchange, in which  $Na^+$  was held in the soil, and  $Ca^{2+}$  was released into the GW. The samples with ratios above 1:1 were calcium- and magnesium-enhanced. This suggests that evaporites are a better source of  $Ca^{2+}$  and  $Mg^{2+}$  than carbonates. The  $Ca^{2+} + Mg^{2+}$  interactions of most of the GW samples with  $HCO_3^- + SO_4^{2-}$  did not indicate that carbonate weathering was the primary process in the study area, as shown in Figure 10b). Additionally, the plot of  $Ca^{2+} + Mg^{2+}$  versus  $HCO_3^-$  (Figure 10c) shows an excess of  $Ca^{2+}$  and  $Mg^{2+}$  caused by silicate weathering, which is a key process in releasing  $HCO_3^-$  into the GW [89]. Figure 10d, which displays the ratios of  $SO_4^{2-}/Ca^{2+}$ , supports this. With a coefficient of correlation value of 0.6 between  $SO_4^{2-}$  and  $Ca^{2+}$ , there is a strong association between the two ions as an indication of gypsum and anhydrite dissolution. Most samples were above the equiline 1:1 in the scatter plot between  $Ca^{2+}$  and  $SO_4^{2-}$  (Figure 10d), suggesting that another source of calcium, calcite, and dolomite, was dissolved in the GW [28]. Samples that deviated from the line 1:1 point to a source of  $SO_4^{2-}$  other than agriculture, such as mineral weathering, ion exchange reactions, or mineral processes.

Chloro-alkaline was used to identify if ion exchange or reverse ion exchange had a greater contribution as a controlling mechanism between the minerals in the aquifer and water [90,91]. In general, the CAI values, such as CAI-I and CAI-II, were positive for all water samples (Figure 10e,f), indicating a significant tendency for reverse ion exchange

between  $\text{Na}^+$  and  $\text{K}^+$  in the groundwater of the study area and  $\text{Ca}^{2+}$  and  $\text{Mg}^{2+}$  in the surrounding rock. From the different ionic ratios relationship, The reverse ion exchange was the main controlling process governing the groundwater chemistry.

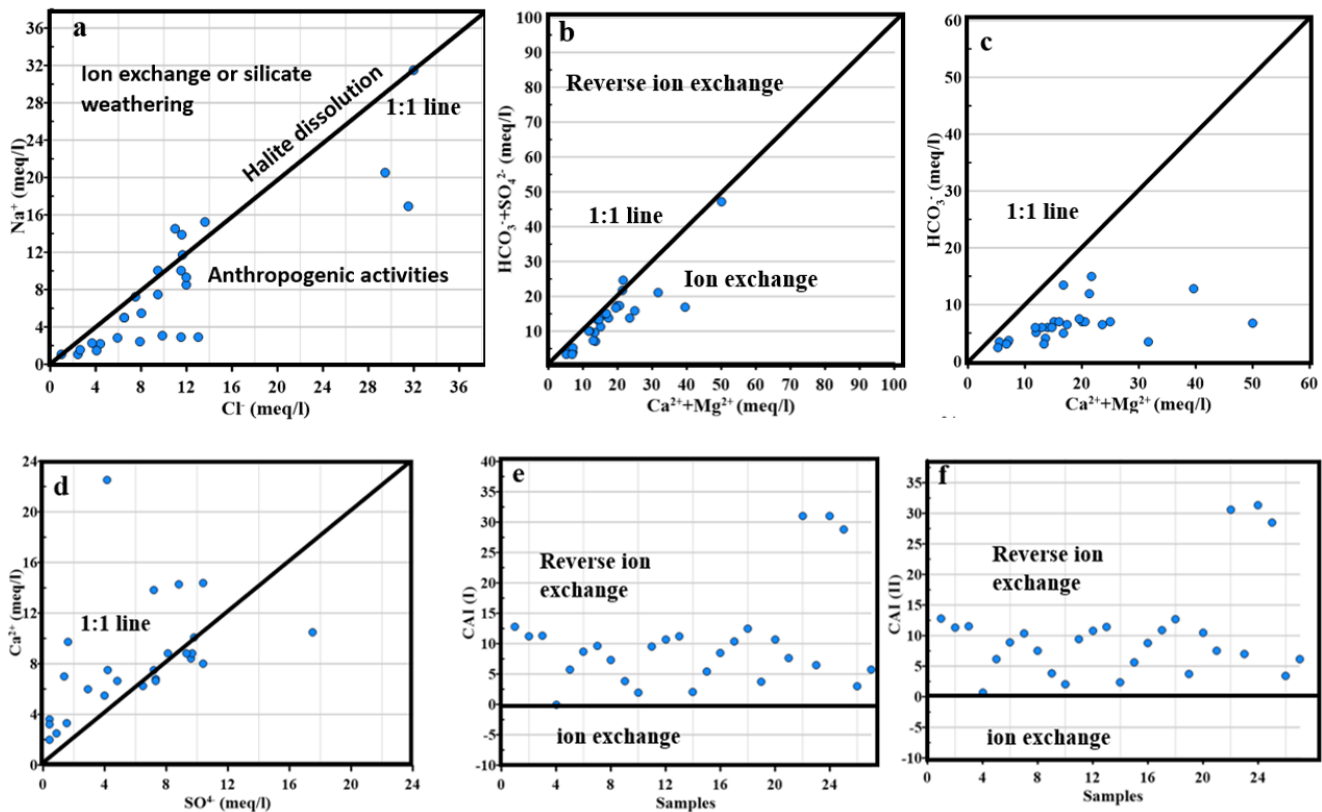


**Figure 10.** Relationships between the main cations and anions in the sample water using stoichiometry: (a)  $\text{Na}^+$  vs.  $\text{Cl}^-$ , (b)  $\text{Ca}^{2+} + \text{Mg}^{2+}$  vs.  $\text{HCO}_3^- + \text{SO}_4^{2-}$ , (c)  $\text{Ca}^{2+} + \text{Mg}^{2+}$  vs.  $\text{HCO}_3^-$ , (d)  $\text{Ca}^{2+}$  vs.  $\text{SO}_4^{2-}$ , (e) Samples vs. CAI-I, and (f) Samples vs. CAI-II.

### 3.3. Statistical Analysis

#### 3.3.1. Cluster Analysis

Integration of the Ward linkage approach and Euclidean distance was used to determine the similarity of the GW samples. A dendrogram is shown in Figure 11 that categorizes the various physicochemical factors in the acquired GW samples. For statistical purposes, standard scores (Z-scores) were obtained for each variable and applied [92]. All variables were logarithmically transformed, and nearly matched normally distributed data were used. Three primary groups have been identified in the dendrogram of the nine physicochemical parameters ( $\text{HCO}_3^-$ ,  $\text{SO}_4^{2-}$ ,  $\text{Cl}^-$ ,  $\text{Mg}^{2+}$ ,  $\text{Ca}^{2+}$ ,  $\text{K}^+$ ,  $\text{Na}^+$ , and TDS) (Figure 11). A specific phenon line was selected at a connection distance of 5, and the specified phenon line [93] was selected. The hydrochemical characteristics of the groups are separated at this distance. Based on the results, the height variables were divided into two clusters managed by the TDS (Figure 11). These are the groups:  $\text{Ca}^{2+}$ ,  $\text{Mg}^{2+}$ ,  $\text{Na}^+$ ,  $\text{K}^+$ , and  $\text{NO}_3^-$  are practically all carbonate components in the compound G1. G2 contains  $\text{SO}_4^{2-}$  and  $\text{Cl}^-$  evaporites. TDS (G3) has two separate sources, the first of which is evaporitic and the second of which is carbonate. The substantial dominance of  $\text{Mg}^{2+}$  and  $\text{Ca}^{2+}$  in the chemical makeup of groundwater, such as sulfates, anhydrite, and calcium sulfates, led to G1, revealing a strong link between the characteristics of the carbonate [94]. However, the G2 showed a strong correlation between evaporite characteristics like  $\text{SO}_4^{2-}$  and  $\text{Cl}^-$ , showing that chlorides and salts were primarily responsible for this groundwater's salinity in the research region. Both G1 and G2 showed that the Quaternary aquifer waters in

Al-Jawf were primarily mineralized owing to their lithological components. Finally, G3 demonstrated that all metrics had varied associations with salinity in this region.

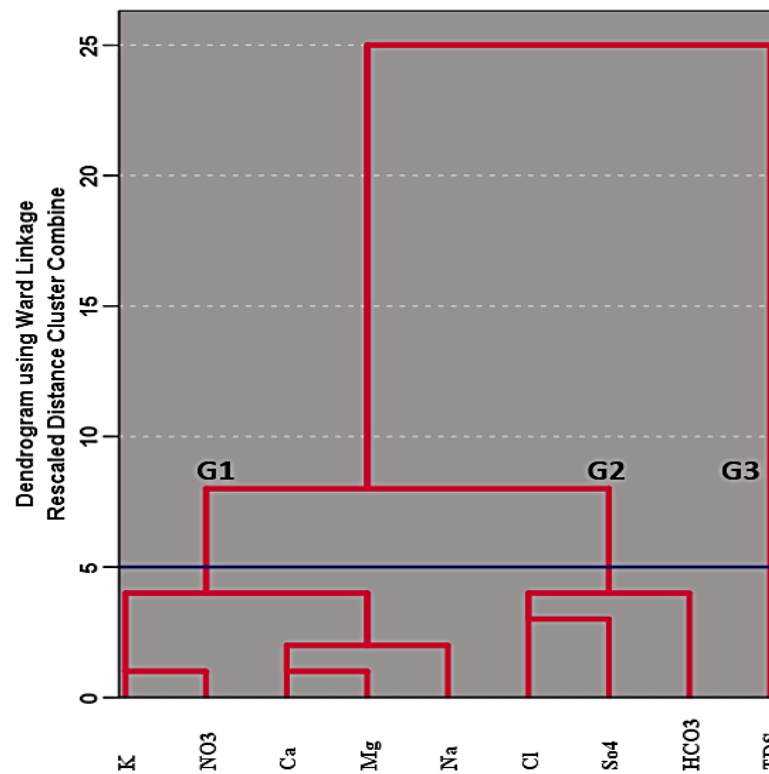


Figure 11. Cluster dendrogram for variables.

### 3.3.2. Principal Component Analysis (PCA)

PCA revealed the retention of three components (F1, F2, and F3) with eigenvalues greater than 1 (Figure 12a). F1 accounted for 55.55% of the variability in the dataset, whereas F2 and F3 accounted for 17.376% and 13.086%, respectively (Figure 12b). Table 4 lists the variable loading values. There was a strong connection between the factors and variables, as indicated by a value close to 1. According to [95], these loads are further divided into three categories: high (>0.75), moderate (from 0.75 to 0.50), and weak (from 0.50 to 0.30). F1 exhibited a strong positive relationship with Mg<sup>2+</sup>, Ca<sup>2+</sup>, Na<sup>+</sup>, Cl<sup>-</sup>, SO<sub>4</sub><sup>2-</sup>, and TDS. Possible sources of SO<sub>4</sub><sup>2-</sup> include oxidation of sulfur compounds and fertilizer-derived SO<sub>4</sub><sup>2-</sup>. However, anthropogenic causes, including irrigation water quality, household waste, and uncontrolled fertilization, may be responsible for Ca<sup>2+</sup>, Na<sup>+</sup>, and Mg<sup>2+</sup>. In addition, the development of salts and soil weathering may have been the cause of the chlorides. A moderate association between F2 and K<sup>+</sup> and a strong correlation between F3 and NO<sub>3</sub><sup>-</sup> indicate that alkaline water moved through the rocks and soil. These findings illuminate the processes through which human behavior occurs.

Table 4. Correlation between the parameters and factors.

Parameters	F1	F2	F3
Ca <sup>2+</sup>	0.770	0.450	0.133
Mg <sup>2+</sup>	0.939	0.196	0.012
Na <sup>+</sup>	0.912	0.191	0.056
K <sup>+</sup>	0.514	0.637	-0.294
HCO <sub>3</sub> <sup>-</sup>	0.176	0.887	0.111

Table 4. Cont.

Parameters	F1	F2	F3
Cl <sup>-</sup>	0.900	0.261	0.192
SO <sub>4</sub> <sup>2-</sup>	0.934	-0.090	-0.235
CO <sub>3</sub> <sup>2-</sup>	0.142	0.375	0.781
TDS	0.944	0.316	0.016
EC	0.955	0.287	0.036
NO <sub>3</sub> <sup>-</sup>	-0.044	-0.205	0.785
Eigenvalue	6.111	1.911	1.439
Variance %	55.556	17.376	13.086
Cumulative	55.556	72.932	86.018

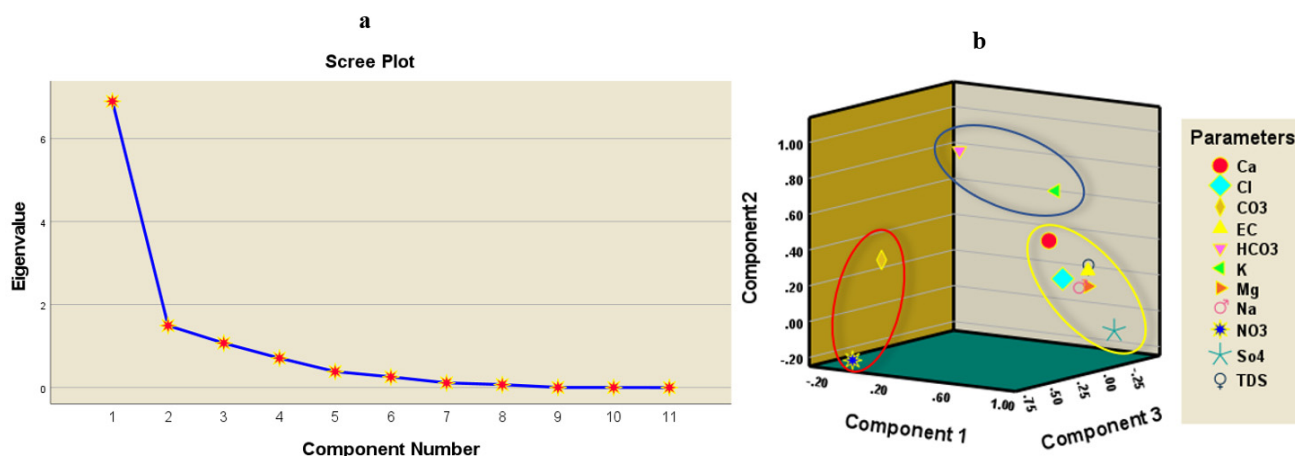


Figure 12. Multivariate statistical analysis: (a), Scree plot and (b) PCA scores for F2 vs. F1 vs. F3.

### 3.4. Geochemical Modeling and Mineral Saturation

The mineral concentrations, saturation indices, and tendency of the GW to dissolve or precipitate minerals were assessed using the PHREEQC model [96]. The model outputs included the saturation indices of relevant minerals such as calcite, dolomite, halite, gypsum, aragonite, and anhydrite, as well as the partial pressure of CO<sub>2</sub>. The input data used included physical and chemical parameters, such as temperature, pH, EC, TDS, and major cations and anions, as shown in Figure 5. The findings for the selected groundwater samples from the Quaternary aquifer are shown in Table 5 and Figure 13. The partial pressure of CO<sub>2</sub> was negative and below saturation, indicating that the amount of water recharged was lower than the quantity of water extracted from the production wells in the Quaternary aquifer. The study also showed that carbon dioxide decreases with the direction of water flow, owing to the same-direction decline in ground water recharging.

Table 5. Statistical description of the mineral SI for the obtained GW samples.

SI	Anhydrite	Aragonite	Calcite	Dolomite	Gypsum	Halite	CO <sub>2</sub> (g)
Min.	-2.79	-0.41	-0.27	-0.29	-2.57	-7.64	-2.32
Max.	-0.44	0.49	0.63	1.45	-0.19	-4.77	-0.63
Mean	-1.501	0.003	0.151	0.404	-1.269	-6.075	-1.649

Water quality can be affected by the presence of various solutes originating from soil erosion, atmospheric deposition, and rock weathering [97]. The dissolution of minerals in water occurs primarily through water-rock interactions, and if water becomes oversaturated with a particular mineral, precipitation can occur [98].

The minimum, maximum, and average SI values for calcite, dolomite, halite, gypsum, aragonite, anhydrite, and CO<sub>2</sub> are listed in Table 5. According to the SI results of the

groundwater in the Quaternary aquifer, all water samples were undersaturated with halite, anhydrite, and gypsum minerals, which means that the GW could dissolve more of these minerals. However, most of the water samples were oversaturated with calcite, dolomite, and aragonite, indicating the possibility of water precipitating these mineral species. This finding is consistent with the Gibbs plot results. Only nine, eight, and 12 samples had negative values for calcite, dolomite, and aragonite, respectively, and these samples were located in the central part of the Al-Jawf area. The semi-arid climate in the study area may have led to the precipitation of dolomite, calcite, and aragonite owing to low rainfall and high evaporation. Calcium, sodium, sulfate, and chloride components are not limited by the mineral equilibrium with anhydrite, gypsum, and halite [99].

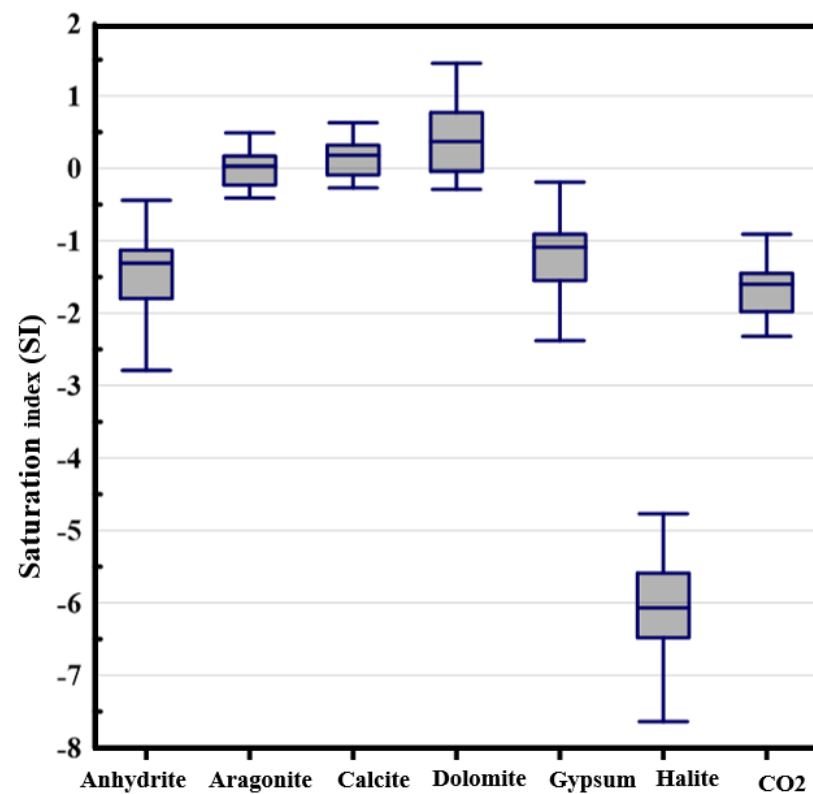


Figure 13. Box plot of the SI results for the Quaternary aquifer in the study area.

### 3.5. Irrigation Water Quality Indices

Several key indicators need to be studied to determine the impact of agricultural soil water quality on the quality of the produced crops. These indicators can either be individual chemical indicators [100,101] or a group of indicators [31,102]. From the results of these indicators, decision-makers can develop an appropriate method for managing irrigation water, which the current study deals with through the following indicators: Considering the typical value intervals for the parameters, the water quality classification for irrigation was applied using the six IWQIs (Table 6).

The IWQI, which was calculated using the equation in Table 1 [31], showed that the water quality in the study area was classified into five criteria [75] and arranged according to the percentage of total samples as follows: 14.8% of samples had a low restriction for irrigation, 14.8% of samples had a moderate restriction for irrigation, 25.9% of samples were highly restricted, and 18.5% of samples were severely restricted, as shown on the map (Figure 14a). The values of the first indicator range from a small value to a maximum value, as shown in Table 6, as follows: 17.03–96.77, with an average of 61.03. Water deterioration, according to the IWQ indicator, was recorded in the far north and southwest of the study area.

**Table 6.** Statistical analysis and classes of IWQIs.

Criteria	Min	Max	Mean	Range	Class	Number of Samples (%)
IWQI	17.03	96.77	61.03	85–100	No restriction	7 (25.920%)
				70–85	Low restriction	4 (14.81%)
				55–70	Moderate restriction	4 (14.81%)
				40–55	High restriction	7 (25.92%)
				0–40	Severe restriction	5 (18.51%)
SAR	0.63	6.30	2.56	<10	Excellent	27 (100%)
				10–18	Good	0 (0%)
				19–26	Fair Poor	0 (0%)
				>26	Unsuitable	0 (0%)
Na%	11.35	49.73	28.29	<20%	Excellent	10 (37%)
				21–40%	Good	13 (48.14%)
				41–60%	Permissible	4 (14.81%)
				61–80%	Doubtful	0 (0%)
				>80%	Unsuitable	50 (100%)
SSP	10.39	49.45	27.57	<60	Suitable	27 (100%)
				>60	Unsuitable	0 (0%)
PS	1.2	52.20	15.23	PS < 3.0	Excellent to good	2 (7.40%)
				PS = 3.0–5.0	Good to injurious	3 (11.11%)
				PS > 5.0	Injurious to unsatisfactory	22 (81.48%)
RCS	−43.21	−1.96	−11.89	<1.25	Good	27 (100%)
				1.25–2.5	Doubtful	0 (0%)
				>2.5	Unsuitable	0 (0%)

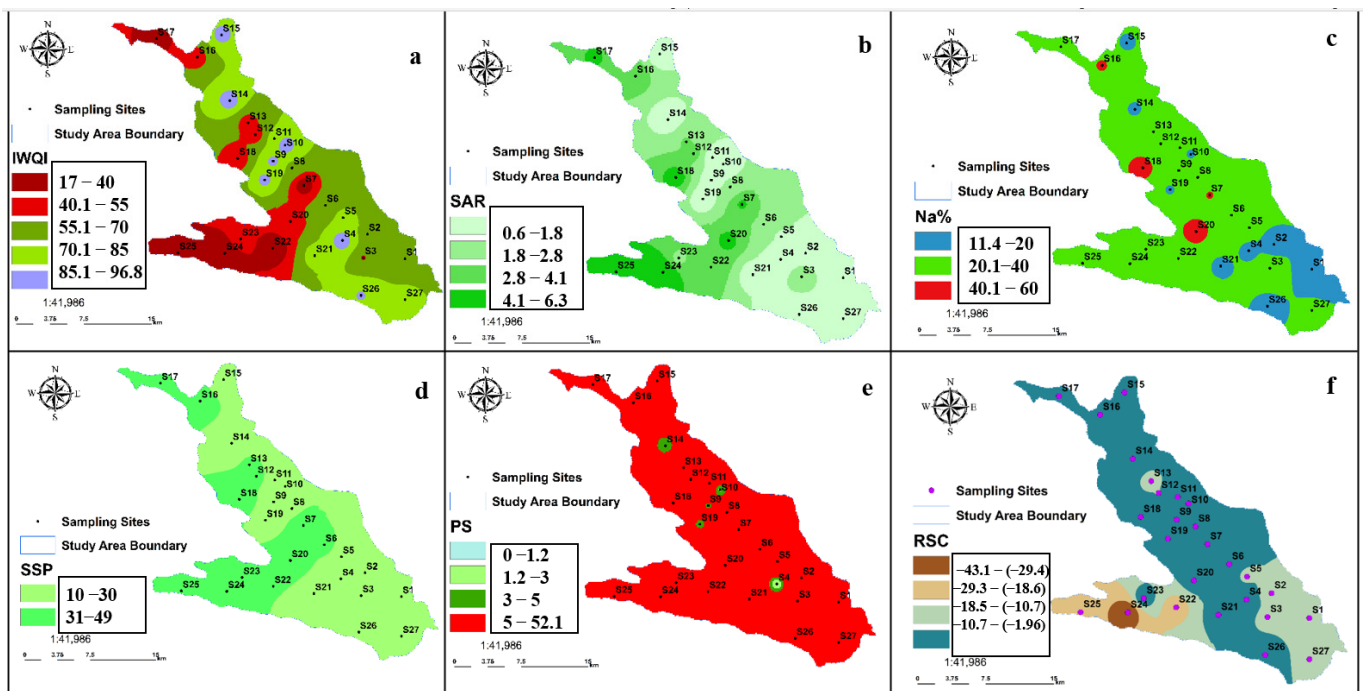


**Figure 14.** The spatial variation maps of the IWQIs for Al-Jawf plain: (a) IWQI, (b) SAR, (c) Na %, (d) SSP, (e) PS, and (f) RSC.

The quality of irrigation water plays an important role in the composition of the soil and its ability to improve or deteriorate agricultural production, as it affects the permeability, rate of filtration, and aeration through the chemical characteristics of irrigation water [103]. Among the constituent elements of water, the concentration of sodium ions is the most

influential on agricultural soils because high concentrations of sodium in irrigation water reduce the filtration rate through soil adsorption of sodium and removal of calcium and magnesium ions [98]. Therefore, SAR, Na%, and SSP indicators were calculated to estimate the water quality through the concentrations of sodium, calcium, and magnesium to determine whether it is suitable for irrigation of agricultural lands [64–66] and to determine the most affected and degraded areas to implement appropriate management to avoid soil degradation. Table 1 shows the method for calculating the four indicators and distributing their values on the maps to determine the areas where soil degradation is expected. The results of the indicators, Table 6, confirmed that all water samples were classified as excellent for the SAR, permissible to excellent for the Na%, and suitable for the SSP index. The average SAR, Na %, and SSP values were 2.56, 28.29, and 27.57%, respectively. From the index distribution maps, Figure 14b–d), it is evident that every sample of water is appropriate for the irrigation of agricultural regions, that there is no negative effect on the soil permeability and infiltration rate, and that there is no need for the application of calcium fertilizers due to the low sodium concentrations in the irrigation water.

The quality of irrigation water can deteriorate in the case of precipitation of alkali elements such as calcium and magnesium. This is due to the increase in the concentration of carbonates in relation to calcium and magnesium in the irrigation water. The concentration of sodium ions increased, followed by an increase in the sodium absorption ratio in the irrigation water due to the precipitation of calcium and magnesium ions in the form of carbonate minerals. Therefore, it is necessary to calculate the RSC index, which evaluates whether water is suitable for irrigation because an increase in the concentration of RSC can cause the dissociation of organic matter and deterioration of the physical properties of the soil, ultimately leading to the appearance of black stains on the surface of the soil when it dries [104,105]. The value of the RSC indicator, Table 1, was calculated to determine the probability of calcium and magnesium ion precipitation on soil surface particles and their removal from the soil solution. The results of the indicator in all study samples, Table 6, and its distribution on the map (Figure 14f), confirmed that the water in the study area is suitable for the irrigation of agricultural lands, as all samples belong to a good classification, and the indicator value ranges from  $-43.21$  to  $-1.96$ . Another indicator, the potential salinity index (PS), depends on the calculation of the concentrations of chloride and sulfate ions [67] to assess the suitability of water for the irrigation of agricultural lands. According to its value (Table 6), it is divided into three categories: Excellent to Good ( $PS < 3.0$ ), Good to Injurious ( $PS = 3.0-5.0$ ), and Injurious to Unsatisfactory ( $PS > 5.0$ ). The PS index results showed that two samples belonged to the Excellent to Good classification, three samples belonged to the good class, and 22 samples belonged to the Injurious to unsatisfactory (Figure 14e).

### 3.6. Simulation Model (ANFIS)

Because the ANFIS model makes predictions based on patterns in the data, the first step in ANFIS prediction is to identify the input variables that will be used for the prediction. These variables should be carefully chosen because they have a direct impact on prediction accuracy. Therefore, a correlation analysis between the input data and the desired output was performed to select the best input variable. This step was repeated for each IWQ index (output), as shown in Figure 5. Once the preprocessing was complete, the best-performing model was selected using ANFIS training for each IWQ index. After the training was complete, the model was tested against new data to determine the accuracy of predicting future values. The values of the IWQ indices predicted during the training and testing phases are listed in Table 7. Figures 15–17 show the results of the predictions of IWQI, SAR, and  $CO_2$  in the training and testing phases, respectively. Figures 15–17 show a strong overlap between the predicted and actual values, with some deviations from the measured values. Excellent agreement between the observed and predicted IWQI values as indicated by the high  $R^2$  value ( $>0.95$ ). In terms of performance evaluation metrics for the ANFIS model, the ANFIS model had a good fit for IWQIs in both the training and testing

stages, as evidenced by the E values in Table 7 being over 0.90. The ANFIS model was successfully used in terms of accuracy for all the indices. The performance of the ANFIS model decreased slightly from the training phase to the testing phase, as indicated by the R<sup>2</sup>, RMSE, and MAD values in Table 7. Figures 13 and 14 depict the differences between the predicted and measured IWQIs in the training and testing stages, respectively, as well as the comparative scatter plots. The ANFIS model effectively captured the varying patterns of the observed IWQI data in the time-series plots. The findings of our study support and agree with those of previous studies [38–41,106], which reported that employing the ANFIS model enhanced the prediction accuracy of the standalone model. Overall, the ANFIS is a powerful tool for predictive modeling owing to its ability to capture nonlinear relationships between inputs and outputs while also being able to adapt quickly when new data points are added or removed from the training set.

**Table 7.** Performance criteria of the simulation models for IWQIs prediction.

	Index	Performance Criteria			
		R <sup>2</sup>	RMSE	MAD	E
Training Series	IWQI	0.999	2.393	1.691	0.999
	SAR	0.973	0.098	0.067	0.973
	SSP	0.996	11.202	8.802	0.996
	Anhydrite	0.970	0.003	0.002	0.971
	Aragonite	0.955	0.001	0.001	0.955
	Dolomite	0.988	0.001	0.000	0.980
	Halite	0.985	0.007	0.003	0.980
	Gypsum	0.976	0.002	0.001	0.979
	CO <sub>2</sub>	0.980	0.002	0.001	0.985
Testing Series	IWQI	0.960	5.670	3.665	0.949
	SAR	0.940	0.479	0.222	0.868
	SSP	0.892	11.667	9.880	0.864
	Anhydrite	0.895	0.354	0.159	0.775
	Aragonite	0.908	0.071	0.032	0.886
	Dolomite	0.878	0.318	0.114	0.443
	Halite	0.932	0.860	0.275	0.070
	Gypsum	0.964	0.174	0.056	0.958
	CO <sub>2</sub>	0.879	0.019	0.007	0.999

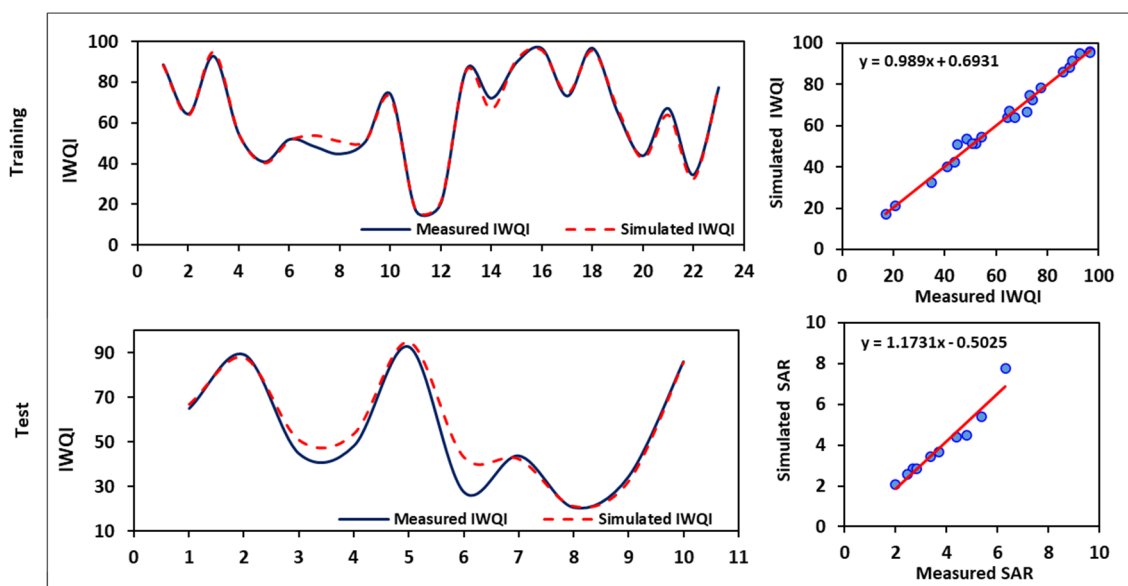


**Figure 15.** Results of the ANFIS model-based simulated IWQI.

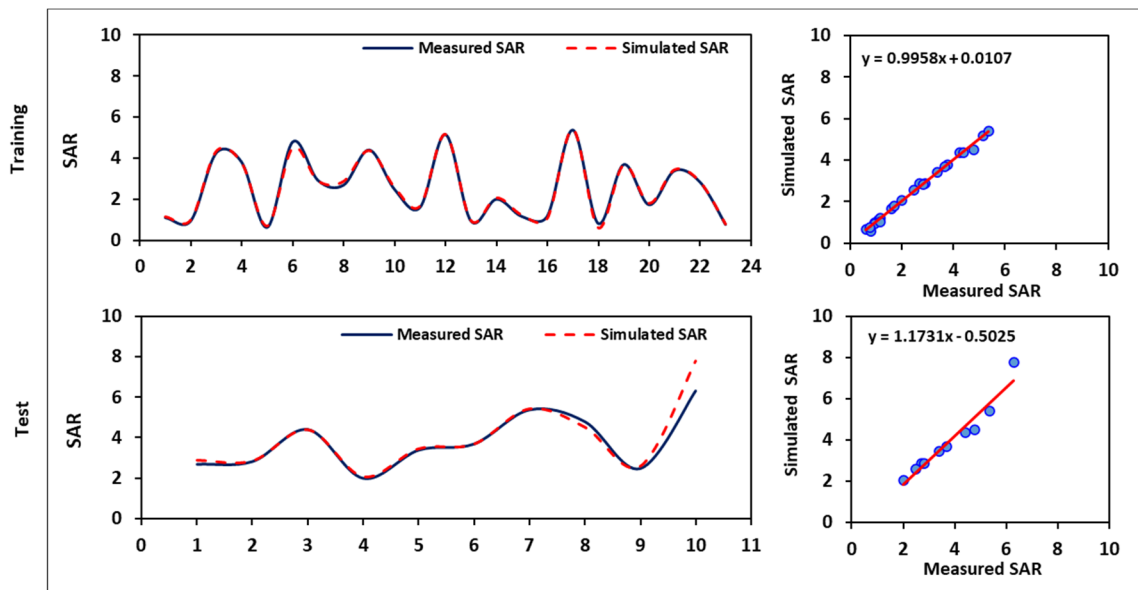


Figure 16. Results of the ANFIS model-based simulated SAR.

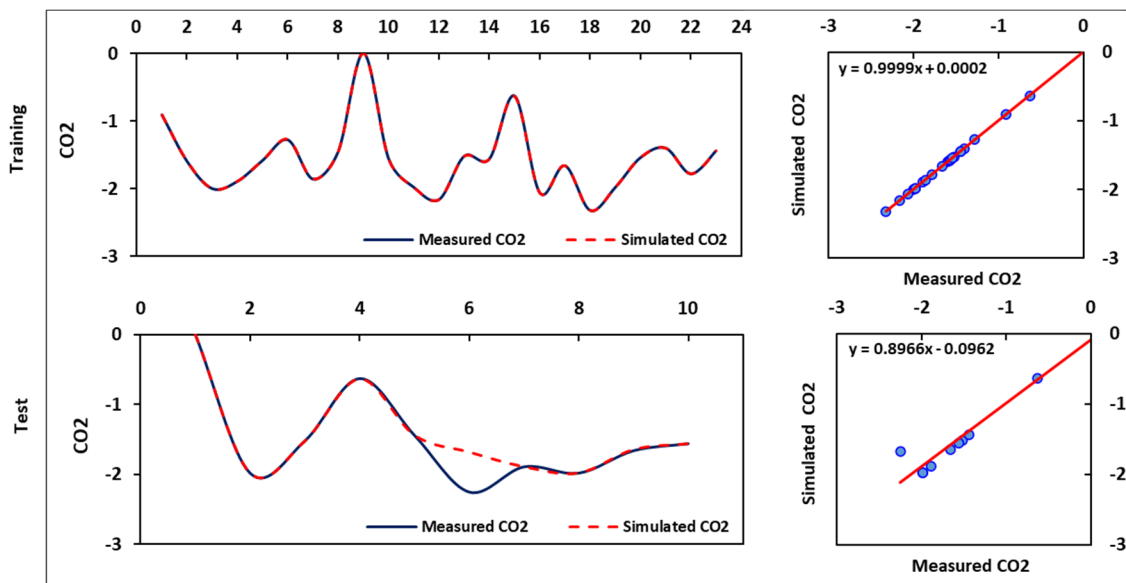


Figure 17. Results of the ANFIS model-based simulated CO<sub>2</sub>.

#### 4. Conclusions

In this study, water quality for irrigation across the Quaternary aquifer in the Al-Jawf Basin, Yemen, was assessed using multivariate statistical analysis, geochemical modeling, IWQIs, ANFIS, and GIS techniques. The results of the physicochemical analysis showed that the GWin in the study area had the following ion sequences:  $Ca^{2+} > Mg^{2+} > Na^{+} > K^{+}$  and  $SO_4^{2-} > Cl^{-} > HCO_3^{-} > NO_3^{-}$ , indicating that the water types were Mg-Ca-Cl/SO<sub>4</sub> and Ca-Mg-HCO<sub>3</sub> because of the predominance of sandstone, limestone, and clay minerals under the influence of human activities, rock weathering, ion dissolution, and direct and reverse ion exchange. This was performed using multivariate statistical analysis. The primary conclusion was that the PCA demonstrated the three most crucial components, with an overall variance of 86.018%. Factors 1, 2, and 3 are, respectively, 55.556%, 17.376%, and 13.086%. The findings demonstrated a substantial relationship between the variables and factors. These findings suggest that the chemical composition is influenced by geochemical characteristics such as the interaction of water and rock and the dissolution of evaporat-

ing mineral deposits. However, the PCA revealed that these two groups were under the supervision of TDS and EC. High correlations between  $\text{Ca}^{2+}$ ,  $\text{Mg}^{2+}$ ,  $\text{Na}^+$ ,  $\text{K}^+$ , and  $\text{NO}_3^-$  were observed in G1. G2 is represented by  $\text{SO}_4^{2-}$  and  $\text{Cl}^-$  atoms and is supported by the evaporite component. The SI value revealed that the GW was supersaturated with calcite, dolomite, and aragonite, providing the ability of water to precipitate these minerals. Halite, gypsum, and anhydrite remain undersaturated, and water can dissolve these minerals. The IWQI results showed that 25.9% of the samples had no restriction for irrigation, 14.8% had a low restriction for irrigation, 14.8% had a moderate restriction for irrigation, 25.9% were highly restricted, and 18.5% were severely restricted. However, the findings obtained using other techniques, such as SAR, Na%, SSP, and RSC, indicated that they ranged from good to excellent, except for the PS method, which revealed outcomes of 2% (great), 3% (good to harmful), and 22% (injurious to unsatisfactory). An evaluation of the ANFIS simulation model demonstrated that it could accurately simulate IWQIs. For example, the IWQI can be predicted with reasonable overall accuracy in both the learning ( $R^2 = 0.980$ ) and validation phases ( $R^2 = 0.916$ ). Therefore, combining physicochemical parameters, IWQIs, ANFIS, and GIS approaches is efficient and provides a complete picture of the appropriateness of GW for irrigation and its controlling factors. Furthermore, the techniques proposed in this study should be further investigated to enhance their reliability for GW under various conditions and encourage decision-makers to implement different technologies for water quality planning and management.

**Author Contributions:** Conceptualization, M.H.E., M.H.A.-M., O.S., M.K., M.F., M.G. and S.E.; fieldwork, M.H.A.-M.; O.S., M.S.A. and M.A.A.; methodology, M.H.E.; M.G., S.E., A.A.A., P.S., A.S., M.R.A. and H.S.R.; software, P.S., M.H.E., M.R.A., A.A.A., H.S.R., M.G., S.E., M.F. and A.S.; validation, M.K., M.F., S.E., O.S., M.H.E. and M.G.; formal analysis, M.S.A., M.H.A.-M., M.R.A., A.A.A., M.H.E. and M.F.; investigation, M.G., M.H.E., O.S., M.R.A., M.S.A., M.A.A. and M.F.; resources, M.H.A.-M., M.A.A., O.S., M.S.A. and M.G.; data curation, S.E., M.R.A., A.S., P.S., A.A.A. and H.S.R., writing original draft preparation, M.H.E.; M.G., M.F., M.K. and S.E.; writing-review and editing, A.S., M.G., P.S., M.H.E. and M.R.A., supervision, P.S., M.H.A.-M., A.A.A., A.S., M.G. and M.R.A.; project administration, M.H.A.-M., M.R.A. and A.A.A. All authors have read and agreed to the published version of the manuscript.

**Funding:** This research received no external funding.

**Institutional Review Board Statement:** Not applicable.

**Informed Consent Statement:** Not applicable.

**Data Availability Statement:** All data are provided as tables and figures.

**Acknowledgments:** The authors extend their appreciation to Renewable Natural Resources Research Center, Agricultural Research and Extension Authority, Dhamar, Yemen, for supporting this work.

**Conflicts of Interest:** The authors declare that they have no known competing financial interest or personal relationships that could have appeared to influence the work reported in this paper.

## References

1. Siebert, S.; Burke, J.; Faures, J.M.; Frenken, K.; Hoogeveen, J.; Döll, P.; Portmann, F.T. Groundwater Use for Irrigation—A Global Inventory. *Hydrol. Earth Syst. Sci.* **2010**, *14*, 1863–1880. [CrossRef]
2. Wang, D.; Wu, J.; Wang, Y.; Ji, Y. Finding High-Quality Groundwater Resources to Reduce the Hydatidosis Incidence in the Shiqu County of Sichuan Province, China: Analysis, Assessment, and Management. *Expo. Health* **2020**, *12*, 307–322. [CrossRef]
3. Salam, M.A.; Adlii, A.; Eid, M.H.; Abukhadra, M.R. Effective Decontamination of  $\text{Ca}^{2+}$  and  $\text{Mg}^{2+}$  Hardness from Groundwater Using Innovative Muscovite Based Sodalite in Batch and Fixed-Bed Column Studies; Dynamic and Equilibrium Studies. *J. Contam. Hydrol.* **2021**, *241*, 103817. [CrossRef] [PubMed]
4. Zhou, Y.; Li, P.; Chen, M.; Dong, Z.; Lu, C. Groundwater Quality for Potable and Irrigation Uses and Associated Health Risk in Southern Part of Gu'an County, North China Plain. *Environ. Geochem Health* **2021**, *43*, 813–835. [CrossRef]
5. Noori, R.; Maghrebi, M.; Jessen, S.; Bateni, S.M.; Heggy, E.; Javadi, S.; Nouri, M.; Pistre, S.; Abolfathi, S.; AghaKouchak, A. Decline in Iran's Groundwater Recharge. PREPRINT (Version 1) Available at Research Square. 2023. Available online: <https://www.researchsquare.com/article/rs-2608948/v1> (accessed on 26 February 2023).
6. Lichtenthaler, G. Water Conflict and Cooperation in Yemen. *Middle East Rep.* **2010**, *254*, 40.

7. Glass, N. The Water Crisis in Yemen: Causes, Consequences and Solutions. *Glob. Major. E-J.* **2010**, *1*, 17–30.
8. Bigio, A.G.; Licciardi, G. The Urban Rehabilitation of Medinas: The World Bank Experience in the Middle East and North Africa. 2010. Available online: <http://hdl.handle.net/10986/17382> (accessed on 26 February 2023).
9. Abbas, A.A.; Mohamed, H.I.; Ali, N.A. Assessment of Water Resources in Dhamar Governorate, Yemen Republic. In Proceedings of the 9th International Conference for Development and the Environment in the Arab World, Assiut University, Assiut, Egypt, 15–17 April 2018; pp. 15–17.
10. Al-Asbahi, Q.Y.A. Water Resources Information in Yemen. United Nations Intersecretariat Working Group on Environment Statistics (IWG-ENV), International Work Session on Water Statistics, Vienna (June 20–22). 2005. Available online: [http://unstats.un.org/unsd/environment/envpdf/pap\\_wasess3a3yemen](http://unstats.un.org/unsd/environment/envpdf/pap_wasess3a3yemen) (accessed on 26 February 2023).
11. Sultana, H.; Ali, N.; Iqbal, M.M.; Khan, A.M. Vulnerability and Adaptability of Wheat Production in Different Climatic Zones of Pakistan under Climate Change Scenarios. *Clim. Chang.* **2009**, *94*, 123–142. [[CrossRef](#)]
12. Moore, S. Parchedness, Politics, and Power: The State Hydraulic in Yemen. *J. Political Ecol.* **2011**, *18*, 38–50. [[CrossRef](#)]
13. Everest, T.; Özcan, H. Applying Multivariate Statistics for Identification of Groundwater Resources and Qualities in NW Turkey. *Environ. Monit Assess* **2019**, *191*, 47. [[CrossRef](#)]
14. Sajil Kumar, P.J.; James, E.J. Geostatistical and Geochemical Model-Assisted Hydrogeochemical Pattern Recognition along the Groundwater Flow Paths in Coimbatore District, South India. *Environ. Dev. Sustain.* **2019**, *21*, 369–384. [[CrossRef](#)]
15. Gaagai, A. Etude de L'évolution de la Qualité Des Eaux du Barrage de Babar (Sud-Est Algérien) et L'impact de la Rupture de la Digue sur L'environnement. Ph.D. Thesis, Université de Batna, Batna, Algeria, 2017.
16. Elsayed, S.; Hussein, H.; Moghanm, F.S.; Khedher, K.M.; Eid, E.M.; Gad, M. Application of Irrigation Water Quality Indices and Multivariate Statistical Techniques for Surface Water Quality Assessments in the Northern Nile Delta, Egypt. *Water* **2020**, *12*, 3300. [[CrossRef](#)]
17. Gad, M.; El-Hendawy, S.; Al-Suhaibani, N.; Tahir, M.U.; Mubushar, M.; Elsayed, S. Combining Hydrogeochemical Characterization and a Hyperspectral Reflectance Tool for Assessing Quality and Suitability of Two Groundwater Resources for Irrigation in Egypt. *Water* **2020**, *12*, 2169. [[CrossRef](#)]
18. Shakeri, A.; Ghoreyshinia, S.; Mehrabi, B. Surface and Groundwater Quality in Taftan Geothermal Field, SE Iran. *Water Qual. Expo. Health* **2015**, *7*, 205–218. [[CrossRef](#)]
19. Zhai, Y.; Zheng, F.; Zhao, X.; Xia, X.; Teng, Y. Identification of Hydrochemical Genesis and Screening of Typical Groundwater Pollutants Impacting Human Health: A Case Study in Northeast China. *Environ. Pollut.* **2019**, *252*, 1202–1215. [[CrossRef](#)]
20. Piper, A.M. A Graphic Procedure in the Geochemical Interpretation of Water-Analyses. *Trans. AGU* **1944**, *25*, 914. [[CrossRef](#)]
21. Gibbs, R.J. Mechanisms Controlling World Water Chemistry. *Science* **1970**, *170*, 1088–1090. [[CrossRef](#)]
22. Chadha, D.K. A Proposed New Diagram for Geochemical Classification of Natural Waters and Interpretation of Chemical Data. *Hydrogeol. J.* **1999**, *7*, 431–439. [[CrossRef](#)]
23. Gad, M.; Saad, A. Hydrogeochemical Evaluation of Fractured Limestone Aquifer by Applying a Geochemical Model in Eastern Nile Valley, Egypt. *Environ. Earth Sci.* **2017**, *76*, 641. [[CrossRef](#)]
24. Al-Ruwaih, F.M. Hydrogeology and Groundwater Geochemistry of the Clastic Aquifer and Its Assessment for Irrigation, Southwest Kuwait. In *Aquifers-Matrix and Fluids*; Javaid, M.S., Khan, S.A., Eds.; InTech: Gurugram, India, 2018; ISBN 978-1-78923-490-9.
25. Gad, M.; Dahab, K.; Ibrahim, H. Applying of a Geochemical Model on the Nubian Sandstone Aquifer in Siwa Oasis, Western Desert, Egypt. *Environ. Earth Sci.* **2018**, *77*, 401. [[CrossRef](#)]
26. Gaagai, A.; Boudoukha, A.; Boumezbeur, A.; Benaabidate, L. Hydrochemical Characterization of Surface Water in the Babar Watershed (Algeria) Using Environmetric Techniques and Time Series Analysis. *Int. J. River Basin Manag.* **2017**, *15*, 361–372. [[CrossRef](#)]
27. Gad, M.; Abou El-Safa, M.M.; Farouk, M.; Hussein, H.; Alnemari, A.M.; Elsayed, S.; Khalifa, M.M.; Moghanm, F.S.; Eid, E.M.; Saleh, A.H. Integration of Water Quality Indices and Multivariate Modeling for Assessing Surface Water Quality in Qaroun Lake, Egypt. *Water* **2021**, *13*, 2258. [[CrossRef](#)]
28. Athamena, A.; Gaagai, A.; Aouissi, H.A.; Burlakovs, J.; Bencedira, S.; Zekker, I.; Krauklis, A.E. Chemometrics of the Environment: Hydrochemical Characterization of Groundwater in Lioua Plain (North Africa) Using Time Series and Multivariate Statistical Analysis. *Sustainability* **2023**, *15*, 20. [[CrossRef](#)]
29. Nagaraju, A.; Muralidhar, P.; Sreedhar, Y. Hydrogeochemistry and Groundwater Quality Assessment of Rapur Area, Andhra Pradesh, South India. *GEP* **2016**, *4*, 88–99. [[CrossRef](#)]
30. El Osta, M.; Masoud, M.; Alqarawy, A.; Elsayed, S.; Gad, M. Groundwater Suitability for Drinking and Irrigation Using Water Quality Indices and Multivariate Modeling in Makkah Al-Mukarramah Province, Saudi Arabia. *Water* **2022**, *14*, 483. [[CrossRef](#)]
31. Meireles, A.C.M.; de Andrade, E.M.; Chaves, L.C.G.; Frischkorn, H.; Crisostomo, L.A. A New Proposal of the Classification of Irrigation Water. *Rev. Ciênc. Agron.* **2010**, *41*, 349–357. [[CrossRef](#)]
32. Gharbi, A.; Ali, Z.I.; Zairi, M. Groundwater Suitability for Drinking and Agriculture Purposes Using Irrigation Water Quality Index and Multivariate Analysis: Case of Sidi Bouzid Aquifer, Central Tunisia. *Environ. Earth Sci.* **2019**, *78*, 692. [[CrossRef](#)]
33. Khouni, I.; Louhichi, G.; Ghrabi, A. Use of GIS Based Inverse Distance Weighted Interpolation to Assess Surface Water Quality: Case of Wadi El Bey, Tunisia. *Environ. Technol. Innov.* **2021**, *24*, 101892. [[CrossRef](#)]

34. Eid, M.H.; Elbagory, M.; Tamma, A.A.; Gad, M.; Elsayed, S.; Hussein, H.; Moghanm, F.S.; Omara, A.E.-D.; Kovács, A.; Péter, S. Evaluation of Groundwater Quality for Irrigation in Deep Aquifers Using Multiple Graphical and Indexing Approaches Supported with Machine Learning Models and GIS Techniques, Souf Valley, Algeria. *Water* **2023**, *15*, 182. [[CrossRef](#)]
35. Gaagai, A.; Aouissi, H.A.; Bencedira, S.; Hinge, G.; Athamena, A.; Haddam, S.; Gad, M.; Elsherbiny, O.; Elsayed, S.; Eid, M.H.; et al. Application of Water Quality Indices, Machine Learning Approaches, and GIS to Identify Groundwater Quality for Irrigation Purposes: A Case Study of Sahara Aquifer, Doucen Plain, Algeria. *Water* **2023**, *15*, 289. [[CrossRef](#)]
36. Ibrahim, H.; Yaseen, Z.M.; Scholz, M.; Ali, M.; Gad, M.; Elsayed, S.; Khadr, M.; Hussein, H.; Ibrahim, H.H.; Eid, M.H.; et al. Evaluation and Prediction of Groundwater Quality for Irrigation Using an Integrated Water Quality Indices, Machine Learning Models and GIS Approaches: A Representative Case Study. *Water* **2023**, *15*, 694. [[CrossRef](#)]
37. Khadr, M. *Water Resources Management in the Context of Drought (an Application to the Ruhr River Basin in Germany)*; Shaker: Maastricht, The Netherlands, 2011; ISBN 3-8440-0082-8.
38. Khadr, M.; Elshemy, M. Data-Driven Modeling for Water Quality Prediction Case Study: The Drains System Associated with Manzala Lake, Egypt. *Ain Shams Eng. J.* **2017**, *8*, 549–557. [[CrossRef](#)]
39. Khadr, M.; Schlenkhoff, A. Data-Driven Stochastic Modeling for Multi-Purpose Reservoir Simulation. *J. Appl. Water Eng. Res.* **2018**, *6*, 40–47. [[CrossRef](#)]
40. Khadr, M.; Gad, M.; El-Hendawy, S.; Al-Suhaibani, N.; Dewir, Y.H.; Tahir, M.U.; Mubushar, M.; Elsayed, S. The Integration of Multivariate Statistical Approaches, Hyperspectral Reflectance, and Data-Driven Modeling for Assessing the Quality and Suitability of Groundwater for Irrigation. *Water* **2020**, *13*, 35. [[CrossRef](#)]
41. Khadr, M.; Schlenkhoff, A. GA-Based Implicit Stochastic Optimization and RNN-Based Simulation for Deriving Multi-Objective Reservoir Hedging Rules. *Environ. Sci. Pollut. Res.* **2021**, *28*, 19107–19120. [[CrossRef](#)]
42. Alquraish, M.; Abuhasel, K.A.; Alqahtani, A.S.; Khadr, M. SPI-Based Hybrid Hidden Markov–GA, ARIMA–GA, and ARIMA–GA–ANN Models for Meteorological Drought Forecasting. *Sustainability* **2021**, *13*, 12576. [[CrossRef](#)]
43. Alquraish, M.M.; Abuhasel, K.A.; Alqahtani, A.S.; Khadr, M. A Comparative Analysis of Hidden Markov Model, Hybrid Support Vector Machines, and Hybrid Artificial Neural Fuzzy Inference System in Reservoir Inflow Forecasting (Case Study: The King Fahd Dam, Saudi Arabia). *Water* **2021**, *13*, 1236. [[CrossRef](#)]
44. Khadr, M.; Schlenkhoff, A. Integration of Data-Driven Modeling and Stochastic Modeling for Multi-Purpose Reservoir Simulation. In Proceedings of the 11th International Conference on Hydroscience & Engineering, Hamburg, Germany, 28 September–2 October 2014; pp. 91–100.
45. Karunanidhi, D.; Subramani, T.; Roy, P.D.; Li, H. Impact of Groundwater Contamination on Human Health. *Environ. Geochem. Health* **2021**, *43*, 643–647. [[CrossRef](#)]
46. Fuoco, I.; Marini, L.; De Rosa, R.; Figoli, A.; Gabriele, B.; Apollaro, C. Use of Reaction Path Modelling to Investigate the Evolution of Water Chemistry in Shallow to Deep Crystalline Aquifers with a Special Focus on Fluoride. *Sci. Total Environ.* **2022**, *830*, 154566. [[CrossRef](#)]
47. Ministry of National Planning and Economic Development. Yearbook, S. Central Statistical Organization. 1995.
48. Al-Shamiry, F.M.S. Agricultural Mechanization Development in Yemen (1970–2003). 2020. Available online: <https://ijpsat.org/index.php/ijpsat/article/view/2078> (accessed on 26 February 2023).
49. Alaug, A.S.; Al-Wosabi, K.A. Organic Geochemical Evaluation of Madbi Source Rock, Al-Jawf Basin, NE Central Yemen. *Iran. J. Earth Sci.* **2015**, *7*, 25–36.
50. Hem, J.D. *Study and Interpretation of the Chemical Characteristics of Natural Water*; Department of the Interior, US Geological Survey: Reston, VA, USA, 1985; Volume 2254.
51. Rodier, J. *L'analyse de L'eau: Eaux Naturelles, Eaux Résiduelles, Eau de Mer: Chimie, Physico-Chimie, Bactériologie, Biologie*, 7th ed.; Dunod: Paris, France, 1984; ISBN 978-2-04-015615-2.
52. Lima, V.R.d.N.; Silva, Á.G.F.d.; Cruz, R.R.P.; Barbosa, L.d.S.; Junior, N.R.d.S.; Sales, G.N.B.; Limão, M.A.R.; Costa, F.B.d.; Souza, P.A.d.; Lopes, K.P.; et al. Nopalea Cochenillifera Biomass as Bioadsorbent in Water Purification. *Water* **2021**, *13*, 2012. [[CrossRef](#)]
53. Szekely, E. A Rapid Colorimetric Method for Analysis of Nitrate Nitrogen by Reduction to Nitrite. *Commun. Soil Sci. Plant Anal.* **1991**, *22*, 1295–1302. [[CrossRef](#)]
54. Chen, K.; Yu, S.; Ma, T.; Ding, J.; He, P.; Li, Y.; Dai, Y.; Zeng, G. Modeling the Water and Nitrogen Management Practices in Paddy Fields with HYDRUS-1D. *Agriculture* **2022**, *12*, 924. [[CrossRef](#)]
55. Cho, Y.-C.; Choi, H.; Lee, M.-G.; Kim, S.-H.; Im, J.-K. Identification and Apportionment of Potential Pollution Sources Using Multivariate Statistical Techniques and APCS-MLR Model to Assess Surface Water Quality in Injin River Watershed, South Korea. *Water* **2022**, *14*, 793. [[CrossRef](#)]
56. Barkat, A.; Bouaicha, F.; Bouteraa, O.; Mester, T.; Ata, B.; Balla, D.; Rahal, Z.; Szabó, G. Assessment of Complex Terminal Groundwater Aquifer for Different Use of Oued Souf Valley (Algeria) Using Multivariate Statistical Methods, Geostatistical Modeling, and Water Quality Index. *Water* **2021**, *13*, 1609. [[CrossRef](#)]
57. Chounlamany, V.; Tanchuling, M.A.; Inoue, T. Spatial and Temporal Variation of Water Quality of a Segment of Marikina River Using Multivariate Statistical Methods. *Water Sci. Technol.* **2017**, *76*, 1510–1522. [[CrossRef](#)]
58. Mutea, F.G.; Nelson, H.K.; Au, H.V.; Huynh, T.G.; Vu, U.N. Assessment of Water Quality for Aquaculture in Hau River, Mekong Delta, Vietnam Using Multivariate Statistical Analysis. *Water* **2021**, *13*, 3307. [[CrossRef](#)]

59. Mohanty, C.R.; Nayak, S.K. Assessment of Seasonal Variations in Water Quality of Brahmani River Using PCA. *Adv. Environ. Res.* **2017**, *6*, 53–65. [[CrossRef](#)]
60. Wu, M.-L.; Wang, Y.-S. Using Chemometrics to Evaluate Anthropogenic Effects in Daya Bay, China. *Estuar. Coast. Shelf Sci.* **2007**, *72*, 732–742. [[CrossRef](#)]
61. Yu, S.; Shang, J.; Zhao, J.; Guo, H. Factor Analysis and Dynamics of Water Quality of the Songhua River, Northeast China. *Water Air Soil Pollut.* **2003**, *144*, 159–169. [[CrossRef](#)]
62. Schoeller, H. Methods and Techniques of Groundwater Investigation and Development. *Water Resour. Ser.* **1967**, *33*, 44–52.
63. Appelo, C.A.J.; Postma, D. *Geochemistry, Groundwater and Pollution*; Balkema: Rotterdam, The Netherlands, 1993; p. 536.
64. Richards, L.A. *Diagnosis and Improvement of Saline and Alkali Soils*; LWW: Philadelphia, PA, USA, 1954; Volume 78, ISBN 0038-075X.
65. Ravikumar, P.; Aneesul Mehmood, M.; Somashekar, R.K. Water Quality Index to Determine the Surface Water Quality of Sankey Tank and Mallathahalli Lake, Bangalore Urban District, Karnataka, India. *Appl. Water Sci.* **2013**, *3*, 247–261. [[CrossRef](#)]
66. Eaton, F.M. Significance of Carbonates in Irrigation Waters. *Soil Sci.* **1950**, *69*, 123–134. [[CrossRef](#)]
67. Doneen, L.D. *Water Quality for Agriculture*; Department of Irrigation, University of California: Davis, CA, USA, 1964; p. 48.
68. Zubaidi, S.; Al-Bugharbee, H.; Ortega-Martorell, S.; Gharghan, S.; Olier, I.; Hashim, K.; Al-Bdairi, N.; Kot, P. A Novel Methodology for Prediction Urban Water Demand by Wavelet Denoising and Adaptive Neuro-Fuzzy Inference System Approach. *Water* **2020**, *12*, 1628. [[CrossRef](#)]
69. Veza, I.; Muhamad Said, M.F.; Abdul Latiff, Z.; Abas, M.A. Application of Elman and Cascade Neural Network (ENN and CNN) in Comparison with Adaptive Neuro Fuzzy Inference System (ANFIS) to Predict Key Fuel Properties of ABE-Diesel Blends. *Int. J. Green Energy* **2021**, *18*, 1510–1522. [[CrossRef](#)]
70. Adnan Ikram, R.M.; Jaafari, A.; Milan, S.G.; Kisi, O.; Heddam, S.; Zounemat-Kermani, M. Hybridized Adaptive Neuro-Fuzzy Inference System with Metaheuristic Algorithms for Modeling Monthly Pan Evaporation. *Water* **2022**, *14*, 3549. [[CrossRef](#)]
71. Belvederesi, C.; Dominic, J.A.; Hassan, Q.K.; Gupta, A.; Achari, G. Predicting River Flow Using an AI-Based Sequential Adaptive Neuro-Fuzzy Inference System. *Water* **2020**, *12*, 1622. [[CrossRef](#)]
72. Hassan, H.S.; Abdel Moamen, O.A.; Zaher, W.F. Adaptive Neuro-Fuzzy Inference System Analysis on Sorption Studies of Strontium and Cesium Cations onto a Novel Impregnated Nano-Zeolite. *Adv. Powder Technol.* **2020**, *31*, 1125–1139. [[CrossRef](#)]
73. Vasanthavigar, M.; Srinivasamoorthy, K.; Prasanna, M.V. Evaluation of Groundwater Suitability for Domestic, Irrigational, and Industrial Purposes: A Case Study from Thirumanimuttar River Basin, Tamilnadu, India. *Environ. Monit. Assess.* **2012**, *184*, 405–420. [[CrossRef](#)]
74. Rakotondrabe, F.; Ndam Ngoupayou, J.R.; Mfonka, Z.; Rasolomanana, E.H.; Nyangono Abolo, A.J.; Ako Ako, A. Water Quality Assessment in the Bétaré-Oya Gold Mining Area (East-Cameroon): Multivariate Statistical Analysis Approach. *Sci. Total Environ.* **2018**, *610–611*, 831–844. [[CrossRef](#)]
75. Ayers, R.S.; Westcot, D.W. *Water Quality for Agriculture*; FAO Irrigation and Drainage Paper; Food and Agriculture Organization of the United Nations: Rome, Italy, 1985; ISBN 978-92-5-102263-4.
76. Panno, S.V.; Hackley, K.C.; Hwang, H.H.; Greenberg, S.; Krapac, I.G.; Landsberger, S.; O’Kelly, D.J. Source Identification of Sodium and Chloride Contamination in Natural Waters: Preliminary Results. In Proceedings of the 12th Annual Illinois Groundwater Consortium Symposium, Makanda, IL, USA, 22 April 2002.
77. Mahapatra, D.M.; Satapathy, K.C.; Panda, B. Biofertilizers and Nanofertilizers for Sustainable Agriculture: Phycoproducts and Challenges. *Sci. Total Environ.* **2022**, *803*, 149990. [[CrossRef](#)]
78. Ahmed, I.M.; Ahmed, O.M.; Ozories, M.A. Effect of Sulphur Application and Water Salinity on Soil and Plant Properties. *J. Soil Sci. Environ. Manag.* **2019**, *10*, 29–38. [[CrossRef](#)]
79. Baragaño, D.; Boente, C.; Rodríguez-Valdés, E.; Fernández-Braña, A.; Jiménez, A.; Gallego, J.L.R.; González-Fernández, B. Arsenic Release from Pyrite Ash Waste over an Active Hydrogeological System and Its Effects on Water Quality. *Environ. Sci. Pollut. Res.* **2020**, *27*, 10672–10684. [[CrossRef](#)] [[PubMed](#)]
80. Jain, C.K.; Sharma, S.K.; Singh, S. Physico-Chemical Characteristics and Hydrogeological Mechanisms in Groundwater with Special Reference to Arsenic Contamination in Barpeta District, Assam (India). *Environ. Monit. Assess.* **2018**, *190*, 417. [[CrossRef](#)] [[PubMed](#)]
81. Maghrebi, M.; Noori, R.; Partani, S.; Araghi, A.; Barati, R.; Farnoush, H.; Torabi Haghighi, A. Iran’s Groundwater Hydrochemistry. *Earth Space Sci.* **2021**, *8*, e2021EA001793. [[CrossRef](#)]
82. Thilagavathi, R.; Chidambaram, S.; Prasanna, M.V.; Thivya, C.; Singaraja, C. A Study on Groundwater Geochemistry and Water Quality in Layered Aquifers System of Pondicherry Region, Southeast India. *Appl. Water Sci.* **2012**, *2*, 253–269. [[CrossRef](#)]
83. Apollaro, C.; Tripodi, V.; Vespasiano, G.; De Rosa, R.; Dotsika, E.; Fuoco, I.; Critelli, S.; Muto, F. Chemical, Isotopic and Geotectonic Relations of the Warm and Cold Waters of the Galatro and Antonimina Thermal Areas, Southern Calabria, Italy. *Mar. Pet. Geol.* **2019**, *109*, 469–483. [[CrossRef](#)]
84. Pant, D.; Keesari, T.; Rishi, M.S.; Sharma, D.A.; Jaryal, A.; Kamble, S.N.; Sinha, U.K. Hydrochemical Evolution of Groundwater in the Waterlogged Area of Southwest Punjab. *Arab. J. Geosci.* **2020**, *13*, 773. [[CrossRef](#)]
85. Li, P.; Wu, J.; Qian, H. Preliminary Assessment of Hydraulic Connectivity between River Water and Shallow Groundwater and Estimation of Their Transfer Rate during Dry Season in the Shidi River, China. *Environ. Earth Sci.* **2016**, *75*, 99. [[CrossRef](#)]
86. Belhadj, M.; Boudoukha, A.; Amroune, A.; Gaagai, A.; Ziani, D. Statistical characterization of groundwater quality of the northern area of the basin of hodna, m’sila. Southeastern algeria. *Larhyss J.* **2017**, *31*, 177–194.

87. Chebotarev, I.I. Metamorphism of Natural Waters in the Crust of Weathering—1. *Geochim. Cosmochim. Acta* **1955**, *8*, 22–48. [[CrossRef](#)]
88. Maghrebi, M.; Noori, R.; Mehr, A.D.; Lak, R.; Darougheh, F.; Razmgir, R.; Farnoush, H.; Taherpour, H.; Moghaddam, S.M.R.A.; Araghi, A.; et al. Spatiotemporal Changes in Iranian Rivers' Discharge. *Elem. Sci. Anthr.* **2023**, *11*, 00002. [[CrossRef](#)]
89. Kumar, S.; Kumar, A.; Prashant; Jha, V.N.; Sahoo, S.K.; Ranjan, R.K. Groundwater Quality and Its Suitability for Drinking and Irrigational Purpose in Bhojpur District: Middle Gangetic Plain of Bihar, India. *Water Supply* **2022**, *22*, 7072–7084. [[CrossRef](#)]
90. Qian, C.; Wu, X.; Mu, W.-P.; Fu, R.-Z.; Zhu, G.; Wang, Z.-R.; Wang, D. Hydrogeochemical Characterization and Suitability Assessment of Groundwater in an Agro-Pastoral Area, Ordos Basin, NW China. *Environ. Earth Sci.* **2016**, *75*, 1356. [[CrossRef](#)]
91. Wu, J.; Li, P.; Qian, H. Hydrochemical Characterization of Drinking Groundwater with Special Reference to Fluoride in an Arid Area of China and the Control of Aquifer Leakage on Its Concentrations. *Environ. Earth Sci.* **2015**, *73*, 8575–8588. [[CrossRef](#)]
92. Güler, C.; Thyne, G.D.; McCray, J.E.; Turner, K.A. Evaluation of Graphical and Multivariate Statistical Methods for Classification of Water Chemistry Data. *Hydrogeol. J.* **2002**, *10*, 455–474. [[CrossRef](#)]
93. Sneath, P.H.A.; Sokal, R.R. *Numerical Taxonomy: The Principles and Practice of Numerical Classification*; A Series of books in biology; W. H. Freeman: San Francisco, CA, USA, 1973; ISBN 978-0-7167-0697-7.
94. Gad, M.; Gaagai, A.; Eid, M.H.; Szűcs, P.; Hussein, H.; Elsherbiny, O.; Elsayed, S.; Khalifa, M.M.; Moghanm, F.S.; Moustapha, M.E.; et al. Groundwater Quality and Health Risk Assessment Using Indexing Approaches, Multivariate Statistical Analysis, Artificial Neural Networks, and GIS Techniques in El Kharga Oasis, Egypt. *Water* **2023**, *15*, 1216. [[CrossRef](#)]
95. Hinge, G.; Bharali, B.; Baruah, A.; Sharma, A. Integrated Groundwater Quality Analysis Using Water Quality Index, GIS and Multivariate Technique: A Case Study of Guwahati City. *Environ. Earth Sci.* **2022**, *81*, 412. [[CrossRef](#)]
96. Parkhurst, D.L.; Appelo, C.A.J. User's Guide to PHREEQC (Version 2): A Computer Program for Speciation, Batch-Reaction, One-Dimensional Transport, and Inverse Geochemical Calculations. *Water-Resour. Investig. Rep.* **1999**, *99*, 312.
97. Saleh, A.; Al-Ruwaih, F.; Shehata, M. Hydrogeochemical Processes Operating within the Main Aquifers of Kuwait. *J. Arid Environ.* **1999**, *42*, 195–209. [[CrossRef](#)]
98. Pyrcz, M.J.; Deutsch, C.V. *Geostatistical Reservoir Modeling*; Oxford University Press: Oxford, UK, 2014; ISBN 0-19-973144-6.
99. Güler, C.; Thyne, G.D. Hydrologic and Geologic Factors Controlling Surface and Groundwater Chemistry in Indian Wells-Owens Valley Area, Southeastern California, USA. *J. Hydrol.* **2004**, *285*, 177–198. [[CrossRef](#)]
100. Kawo, N.S.; Karuppanan, S. Groundwater Quality Assessment Using Water Quality Index and GIS Technique in Modjo River Basin, Central Ethiopia. *J. Afr. Earth Sci.* **2018**, *147*, 300–311. [[CrossRef](#)]
101. Li, P.; Wu, J.; Qian, H. Assessment of Groundwater Quality for Irrigation Purposes and Identification of Hydrogeochemical Evolution Mechanisms in Pengyang County, China. *Environ. Earth Sci.* **2013**, *69*, 2211–2225. [[CrossRef](#)]
102. RamyaPriya, R.; Elango, L. Evaluation of Geogenic and Anthropogenic Impacts on Spatio-Temporal Variation in Quality of Surface Water and Groundwater along Cauvery River, India. *Environ. Earth Sci.* **2018**, *77*, 2. [[CrossRef](#)]
103. Todd, D.K.; Mays, L.W. *Groundwater Hydrology*; John Wiley & Sons: Hoboken, NJ, USA, 2004; ISBN 0-471-05937-4.
104. Srinivasamoorthy, K.; Gopinath, M.; Chidambaram, S.; Vasanthavigar, M.; Sarma, V.S. Hydrochemical Characterization and Quality Appraisal of Groundwater from Pungar Sub Basin, Tamilnadu, India. *J. King Saud Univ. Sci.* **2014**, *26*, 37–52. [[CrossRef](#)]
105. Kumar, M.; Kumari, K.; Ramanathan, A.; Saxena, R. A Comparative Evaluation of Groundwater Suitability for Irrigation and Drinking Purposes in Two Intensively Cultivated Districts of Punjab, India. *Environ. Geol.* **2007**, *53*, 553–574. [[CrossRef](#)]
106. Elsayed, S.; El-Hendawy, S.; Khadr, M.; Elsherbiny, O.; Al-Suhaibani, N.; Dewir, Y.H.; Tahir, M.U.; Mubushar, M.; Darwish, W. Integration of Spectral Reflectance Indices and Adaptive Neuro-Fuzzy Inference System for Assessing the Growth Performance and Yield of Potato under Different Drip Irrigation Regimes. *Chemosensors* **2021**, *9*, 55. [[CrossRef](#)]

**Disclaimer/Publisher's Note:** The statements, opinions and data contained in all publications are solely those of the individual author(s) and contributor(s) and not of MDPI and/or the editor(s). MDPI and/or the editor(s) disclaim responsibility for any injury to people or property resulting from any ideas, methods, instructions or products referred to in the content.